

1 **Model Comparisons Between Canonical Vine Copulas and Meta-Gaussian**
2 **for Forecasting Agricultural Drought ~~Forecasting~~ over China**

3 Authors: Haijiang Wu^{1,2}, Xiaoling Su^{1,2*}, Vijay P. Singh^{3,4}, Te Zhang², ~~and~~ Jixia Qi², and

4 [Shengzhi Huang⁵](#)

5 Affiliation:

6 ¹*Key Laboratory for Agricultural Soil and Water Engineering in Arid Area of Ministry of Education,*
7 *Northwest A&F University, Yangling, Shaanxi, 712100, China*

8 ²*College of Water Resources and Architectural Engineering, Northwest A&F University, Yangling,*
9 *Shaanxi, 712100, China*

10 ³*Department of Biological and Agricultural Engineering & Zachry Department of Civil and*
11 *Environmental Engineering, Texas A&M University, College Station, TX 77843-2117, USA*

12 ⁴*National Water and Energy Center, UAE University, Al Ain, UAE*

13 ⁵*State Key Laboratory Base of Eco-Hydraulic Engineering in Arid Area, Xi'an University of*
14 *Technology, Xi'an, Shaanxi, 710048, China*

15 *Corresponding Author:

16 Dr. Xiaoling Su, College of Water Resources and Architectural Engineering, Northwest A&F
17 University, Weihui Road 23, Yangling, Shaanxi, China, *Email: xiaolingsu@nwafu.edu.cn* (X. Su).

21 Abstract

22 Agricultural drought is mainly caused by reduced soil moisture and precipitation and ~~affects~~
23 shows adverse impacts on the growth of crops and vegetation, ~~and in turn~~ thus affecting agricultural
24 production and food security. For developing measures for drought mitigation, reliable agricultural
25 drought forecasting is essential. In this study, we developed an agricultural drought forecasting
26 model based on canonical vine copulas under three-dimensions (3C-vine model), in which the
27 antecedent meteorological drought and agricultural drought persistence were utilized as predictors.
28 Besides, the meta-Gaussian (MG) model was selected as a reference model to evaluate the forecast
29 skill. The agricultural drought in August of 2018 was selected as a typical case study, and the spatial
30 patterns of 1–3-month lead forecasts of agricultural drought utilizing the 3C-vine model resembled
31 the corresponding observations, indicating the good predictive ability of the model. The performance
32 metrics (NSE, R^2 , and RMSE) showed that the 3C-vine model outperformed the MG model for
33 forecasting agricultural drought in August under diverse lead times. Also, the 3C-vine model
34 exhibited excellent forecast skills in capturing the extreme agricultural drought over different
35 selected typical regions. This study may help ~~with to~~ guide drought early warning, drought
36 mitigation, and water resources scheduling.

37 **Keywords:** ~~agricultural~~ drought forecasting, model comparison, vine copulas, meta-Gaussian

38 1. Introduction

39 Agriculture is the source of livelihoods of over 2.5 billion people worldwide, and the
40 agricultural sector also sustains 82% of all drought impacts (FAO, 2021). A cascade of impacts of
41 droughts, such as crop reduction and failure, increased human and tree mortality, and ecological
42 disturbance, have attracted considerable attention (FAO, 2021; Lu et al., 2012; Modanesi et al., 2020;

43 Su et al., 2018; Zhang et al., 2018; Zhang et al., 2019; Zscheischler et al., 2020). Droughts have
44 reduced global crop production by about 9–10% for the period 1964–2007 (Lesk et al., 2016).
45 Additionally, droughts have caused overall crop and livestock production loss of \$37 billion over
46 the least developed and lower-middle-income countries (FAO, 2021). Agricultural drought
47 forecasting, therefore, lies at the core of overall drought risk management and is critical for food
48 security, early warning, ~~and as well as~~ drought [preparedness and](#) mitigation.

49 Agricultural drought is generally referred to as soil moisture shortage, which [adversely](#) affects
50 crop yield and vegetation health (Modanesi et al., 2020; Zhang et al., 2016; Zhang et al., 2021).
51 Under natural conditions, atmospheric precipitation is a paramount source for replenishment of soil
52 moisture (Wu et al., 2021a). Therefore, reduced soil moisture (agricultural drought) ~~is~~ mainly [arise](#)
53 [from](#) ~~due to~~ precipitation deficit (meteorological drought) (Modanesi et al., 2020; Orth ~~&~~ [and](#)
54 Destouni, 2018). Moreover, soil moisture has a good memory to drought because of the time-
55 integration effects (Long et al., 2019), i.e., agricultural drought persistence. ~~The p~~Previous
56 meteorological drought and antecedent agricultural drought can be taken into consideration as
57 predictors of subsequent agricultural drought.

58 In hydrology, [some physically-based hydrological models \(e.g., Distributed Time-Variant Gain](#)
59 [Hydrological Model \(DTVGM; Ma et al, 2021\) and Soil and Water Assessment Tool \(SWAT; Wu et](#)
60 [al., 2019\)\) are widely used in hydrological simulation and prediction, the droughts included as well.](#)
61 [However, the physically-based hydrological models typically apply to a catchment or sub-regional](#)
62 [scale, and generally require numerous hydrometeorological variables to achieve more accurate real-](#)
63 [time predictions \(Liu et al., 2021a; Xu et al., 2021a\).](#) ~~the t~~Traditional methods, [such as regression](#)
64 [models, machine learning models, and hybrid models \(by considering both statistical and dynamical](#)

65 [predictions](#)) ([Hao et al., 2016](#)), have been extensively employed to forecast drought, ~~such as~~
66 ~~regression models, machine learning models, and hybrid models (by considering both statistical and~~
67 ~~dynamical predictions)~~ (~~Hao et al., 2016~~). Yet, these models tend to be limited in considering the
68 complex nonlinear (e.g., regression models), explicit physical mechanisms and over-fitting (e.g.,
69 machine learning models), as well as the demand of massive hydroclimatic data input (e.g., hybrid
70 models). The copula functions overcome the limitations of ~~the~~ [aforementioned](#) conventional
71 statistical methods. Since copulas ~~can~~ [are](#) flexible joining arbitrary marginal distributions of
72 variables, they have been widely employed in risk assessment ([Hao et al., 2017](#); [Liu et al., 2021b](#);
73 [Sarhadi et al., 2016](#); [Xu et al., 2021b](#); [Zhang et al., 2021](#); [Zhou et al., 2019](#)), flood and runoff
74 forecasting ([Bevacqua et al., 2017b](#); [Hemri et al., 2015](#); [Liu et al., 2018](#); [Zhang & Singh, 2019](#)),
75 and drought forecasting ([Ganguli & Reddy, 2014](#); [Wu et al., 2021a](#)). However, when bivariate
76 copulas are extended to higher-dimensional (\geq three-dimensions) cases, they are restricted due to
77 nonexistence of analytical expressions ([Liu et al., 2021a](#)). Symmetric Archimedean copulas and
78 nested Archimedean copulas partially have addressed the issues of dimensionality, but single
79 parameter and Archimedean class are difficult to characterize the various dependence structures ([Aas](#)
80 [& Berg, 2009](#); [Hao et al., 2016](#); [Wu et al., 2021a](#)). Fortunately, the vine copulas addressed these
81 limitations ([Aas et al., 2009](#); [Bedford & Cooke, 2002](#); [Joe, 1996](#)).

82 Vine copulas are flexible in decomposing any multi-dimensional joint distribution into a
83 hierarchy of bivariate copulas or pair copula constructions ([Aas et al., 2009](#); [Bedford & Cooke,](#)
84 [2002](#); [Liu et al., 2021a](#); [Vernieuwe et al., 2015](#); [Xiong et al., 2014](#)). These copulas have been
85 extensively applied in the hydrological field ([Bevacqua et al., 2017b](#); [Liu et al., 2021b](#); [Vernieuwe](#)
86 [et al., 2015](#); [Wu et al., 2021a](#)). For instance, [Xiong et al. \(2014\)](#) derived the annual runoff

87 distributions using canonical vine copulas. Liu et al. (2018) developed a framework to investigate
88 compound floods based on canonical vine copulas. Wang et al. (2019) utilized regular vine copulas
89 with historical streamflow and climate drivers to simulate monthly streamflow for the headwater
90 catchment of the Yellow River basin. Liu et al. (2021a) developed a hybrid ensemble forecast model,
91 using the Bayesian model averaging combined canonical vine copulas, to forecast water level. Wu
92 et al. (2021a) proposed an agricultural drought forecast model based on vine copulas under four-
93 dimensional scenarios.

94 The meta-Gaussian (MG) model, a popular statistical model in the hydrometeorological
95 community, has explicit conditional distributions, ~~is capable of joining multiple variables and have~~
96 ~~explicit conditional distributions,~~ which is apt for forecasting and risk assessment purposes (Hao
97 et al., 2016; Hao et al., 2019a; Wu et al., 2021b; Zhang et al., 2021). The forecast skills of the MG
98 model for drought or compound dry-hot events, for example, outperformed the persistence-based or
99 random forecast models (Hao et al., 2016; Hao et al., 2019a; Wu et al., 2021b). However, the MG
100 model only depicts the linear relationship among explanatory variables (predictors) and forecasted
101 variable via covariate matrix, it cannot characterize the nonlinear or tail dependence existing in the
102 variables (Hao et al., 2016). Fortunately, Vine copulas can flexibly combine multiple variables via
103 bivariate copula to characterize numerous or complex dependencies. ~~For example, the forecasting of~~
104 ~~compound dry-hot events in summer over Southern Africa was investigated, based on the MG model~~
105 ~~under 1-month and 3-month lead times (Hao et al., 2019).~~ The propagation between meteorological
106 ~~drought and agricultural drought was characterized via the MG model (Xu et al., 2021).~~ However,
107 ~~there~~ There has been a rather limited investigation, to our knowledge, that ~~carrying out~~ conducting
108 model comparisons between vine copulas and MG for agricultural drought forecasting under the

109 same conditions. Therefore, [investigations on drought forecasting skills between vine copulas and](#)
110 [the MG model are needed to obtain more reliable drought forecasts.](#)~~the MG model was selected as~~
111 ~~a competition (or reference) model.~~

112 The objective of this study therefore was to compare the forecast ability of agricultural drought
113 in August of every year in the period 1961–2018 between canonical vine copulas (i.e., 3C-vine
114 model) and MG model under three-dimensional scenario. In the following, we briefly describe the
115 study area and data used in Section 2. The MG and 3C-vine models and performance metrics utilized
116 are presented in Section 3. Results of the 3C-vine model application and assessment are ~~given~~
117 [displayed](#) in Section 4. Finally, the discussion and conclusions are presented in Section 5.

118 2. Study area and data used

119 China stretches across a vast area covering diverse climate regimes and is a major agricultural-
120 producing country (Wu et al., 2021a; Zhang et al., 2015). For the convenience of analyzing spatial
121 patterns of agricultural drought, the climate of China was divided into seven sub-climate regions on
122 the basis of [Zhao \(1983\)](#)~~Yao et al. (2018)~~ and ~~Yao et al. (2018)~~[Zhao \(1983\)](#), as shown in Figure 1.
123 For each sub-climate region, the temperature and moisture conditions when combined are roughly
124 similar, and the type of soil and vegetation have a certain common characteristic (Zhao, 1983).

125 -----**Figure 1.**-----

126 In this study, the gridded monthly precipitation with a $0.25^\circ \times 0.25^\circ$ spatial resolution was
127 obtained from the CN05.1 dataset for the 1961–2018 period over the mainland of China (excluding
128 the Taiwan province), which was provided by the China National Climate Center. The Copernicus
129 Climate Change Service (C3S) at European Center for Medium-Range Weather Forecast (ECMWF)

130 has begun the release of the ERA5 back extension data covering the period 1950–1978 on the
131 Climate Data Store (CDS). Therefore, the gridded monthly soil moisture with a $0.25^\circ \times 0.25^\circ$ spatial
132 resolution corresponding to three soil depths (0–7 cm, 7–28 cm, and 28–100 cm) are available from
133 the ECMWF ERA5 reanalysis datasets for 1961–1978:
134 [https://cds.climate.copernicus.eu/cdsapp#!/dataset/reanalysis-era5-single-levels-monthly-means-
135 preliminary-back-extension?tab=overview](https://cds.climate.copernicus.eu/cdsapp#!/dataset/reanalysis-era5-single-levels-monthly-means-preliminary-back-extension?tab=overview) and 1979–2018:
136 [https://cds.climate.copernicus.eu/cdsapp#!/dataset/reanalysis-era5-single-levels-monthly-
137 means?tab=overview](https://cds.climate.copernicus.eu/cdsapp#!/dataset/reanalysis-era5-single-levels-monthly-means?tab=overview). The CN05.1 and ERA5 reanalysis datasets have been extensively utilized
138 numerous studies, e.g., drought monitoring and forecasting (Wu et al., 2021a; Zhang et al., 2021),
139 long-term climatic analysis (He et al., 2021; Wu et al., 2017), and flash drought attribution analysis
140 (Wang & Yuan, 2021).

141 3. Methodology

142 ~~We employed~~ The Standardized Precipitation Index (SPI, based on monthly precipitation) and
143 Standardized Soil moisture Index (SSI, based on monthly cumulative soil moisture at ~~top-~~three soil
144 depths), ~~respectively,~~ [is leveraged](#) to characterize meteorological drought and agricultural drought
145 at a 6-month timescale, [respectively](#). The empirical Gringorten plotting position formula (Gringorten,
146 1963) was used to obtain the empirical cumulative probabilities of these two indexes, which were
147 then transformed into standardized variables via the normal quantile transformation. Since
148 meteorological drought is a source of other drought types (e.g., agricultural drought), the antecedent
149 precipitation deficiency (i.e., meteorological drought) has a stronger effect on the subsequent soil
150 moisture deficiency (i.e., agricultural drought). Moreover, soil moisture has a good memory for prior
151 drought, i.e., agricultural drought persistence, which is attributed to the soil porosity characteristics

152 and time-integration effects (Long et al., 2019; Wu et al., 2021a).

153 We attempted to use the prior meteorological drought (SPI_{t-i} ; t denotes the target month (e.g.,
154 August), and i indicates lead time (month)) and agricultural drought persistence (SSI_{t-i}) to forecast
155 the subsequent agricultural drought (SSI_t) based on the canonical vine copulas under three-
156 dimensional scenarios (3C-vine model). We selected the meta-Gaussian (MG) model as a reference
157 model to assess the agricultural drought forecast performance of the 3C-vine model. [Here, the 6-
158 month timescale SPI \(SSI\) in August, which is calculated by the cumulative precipitation \(soil
159 moisture\) from March to August, can indirectly reflect the surplus or deficit situations of water in
160 spring \(March-April-May\) and summer \(June-July-August\) seasons. Furthermore, August is a key
161 growth period for crops \(e.g., anthesis, fruiting, and seed filling\) and vegetation and is also a period
162 with frequent droughts \(Wu et al., 2021a\). Undoubtedly, agricultural drought forecast can be
163 implemented in any month of interest, based on 3C-vine model and MG model.](#) More detailed
164 information is given below.

165 3.1. Meta-Gaussian model under three-dimensional scenarios

166 ~~The m~~Meta-Gaussian (MG) model can effectively combine multiple hydrometeorological
167 variables, which have gained attention for drought forecasting and risk assessment (Hao et al., 2019a;
168 Hao et al., 2019b; Wu et al., 2021b; Zhang et al., 2021). Suppose the series of SPI_{t-i} , SSI_{t-i} , and SSI_t
169 correspond to random variables Y_1 , Y_2 , and Y_3 , respectively, the predictand y_3 under the given
170 conditions of y_1 and y_2 based on the MG model can be expressed as (Wilks, 2014):

$$171 \quad y_3 | (y_1, y_2) \sim N(\mu_{y_3|(y_1, y_2)}, \Sigma_{y_3|(y_1, y_2)}) \quad (1)$$

172 where N signifies the Gaussian distribution function, $\mu_{y_3|(y_1, y_2)}$ denotes the conditional mean,

173 and $\Sigma_{y_3|(y_1, y_2)}$ represents the conditional covariate matrix.

174 Furthermore, we removed the forecast values in a specific year of $y_1, y_2,$ and $y_3,$ which denote
 175 $y_1^{-yr}, y_2^{-yr},$ and $y_3^{-yr},$ respectively. Under this circumstance, the covariate matrix Σ regarding $y_1^{-yr},$
 176 $y_2^{-yr},$ and y_3^{-yr} can be written as:

$$177 \quad \Sigma = Cov \begin{bmatrix} (y_1^{-yr}, y_1^{-yr}) & (y_1^{-yr}, y_2^{-yr}) & (y_1^{-yr}, y_3^{-yr}) \\ (y_2^{-yr}, y_1^{-yr}) & (y_2^{-yr}, y_2^{-yr}) & (y_2^{-yr}, y_3^{-yr}) \\ (y_3^{-yr}, y_1^{-yr}) & (y_3^{-yr}, y_2^{-yr}) & (y_3^{-yr}, y_3^{-yr}) \end{bmatrix} = \begin{bmatrix} C_{11} & C_{12} \\ C_{21} & C_{22} \\ C_{31} & C_{32} \end{bmatrix} \begin{bmatrix} C_{13} \\ C_{23} \\ C_{33} \end{bmatrix} = \begin{bmatrix} \Sigma_{11} & \Sigma_{12} \\ \Sigma_{21} & \Sigma_{22} \end{bmatrix} \quad (2)$$

178 The forecast of specific years, i.e., $y_3^{yr},$ can be derived as (Wilks, 2014):

$$179 \quad y_3^{yr} = \mu_{y_3^{-yr}} + \Sigma_{21} \Sigma_{11}^{-1} \begin{bmatrix} y_1^{yr} - \mu_{y_1^{-yr}} \\ y_2^{yr} - \mu_{y_2^{-yr}} \end{bmatrix} \quad (3)$$

180 where $\mu_{y_1^{-yr}}, \mu_{y_2^{-yr}},$ and $\mu_{y_3^{-yr}}$ represent the mean of $y_1^{-yr}, y_2^{-yr},$ and $y_3^{-yr},$ respectively; y_1^{yr} and
 181 y_2^{yr} denote that y_1 and y_2 provided the forecast information at time $t-i$ in a specific year. [More details](#)
 182 [about forecasting agricultural drought based on the MG model can be found in Figure 3.](#)

183 3.2. Canonical vine copulas model under three-dimensional scenarios

184 Copulas can effectively combine multiple variables without the restriction of marginal
 185 distributions (Nelsen, 2013; Sarhadi et al., 2016; Wang et al., 2019; Xiong et al., 2014). They were
 186 initially utilized for deriving joint distributions of two-dimensional variables, since parameters are
 187 easy to assess and the analytical solution is apt to obtain (Liu et al., 2021a; Sadegh et al., 2017).
 188 However, under higher-dimensional (e.g., $d \geq 3$) scenarios, owing to the limitations of a great deal
 189 of parameters and complexity, the copulas (mainly referred to bivariate copulas) are difficult to
 190 promote and apply (Joe, 2014; Liu et al., 2018; Liu et al., 2021a; Sadegh et al., 2017). To overcome
 191 these limitations, Joe (1996) and Aas et al. (2009) developed vine copulas, a hierarchy of pair copula

192 constructions, for multi-dimensional cases. Vine copulas possess two sub-classes: canonical vine
 193 copulas (C-vine copulas) and drawable vine copulas (D-vine copulas). Here, we mainly employed
 194 the C-vine copulas to establish the forecast model of agricultural drought under three-dimensional
 195 conditions. Undoubtedly, a similar scheme is capable of applying to D-vine copulas.

196 C-vine copulas may have numerous tree structures, especially for the case of higher dimensions,
 197 which are associated with the quantity and ordering of variables (Aas et al., 2009; Liu et al., 2018;
 198 Liu et al., 2021a; Wu et al., 2021a). Also, different ordering of variables affects the estimation of the
 199 parameters of C-vine copulas (Liu et al., 2021a; Wang et al., 2019). Given the ordering of variables
 200 Y_1 , Y_2 , and Y_3 for three-dimensional C-vine copula model (termed as 3C-vine model hereinafter;
 201 Figure 2a), the joint probability density function (PDF), g_{123} , can be expressed as (Aas et al., 2009):

$$202 \quad g_{123} = g_1 \bullet g_2 \bullet g_3 \bullet c_{12} \bullet c_{13} \bullet c_{23|1} \quad (4)$$

203 where g_1 , g_2 , and g_3 correspond to the margin density functions of $g_1(y_1)$, $g_2(y_2)$, and $g_3(y_3)$,
 204 respectively; c is the bivariate copula density; c_{12} , c_{13} , and $c_{23|1}$ signify the abbreviation of $c_{1,2}[G_1(y_1)$,
 205 $G_2(y_2)]$, $c_{1,3}[G_1(y_1)$, $G_3(y_3)]$, and $c_{2,3|1}[G(y_2|y_1)$, $G(y_3|y_1)]$, respectively. [The Gaussian \(or Normal\),
 206 Student-t, Clayton, and Frank copulas, as well as their rotated \(survival\) forms \(Dißmann et al., 2013;
 207 Liu et al., 2021b\) are utilized to obtain the optimal internal bivariate copulas for distinct trees in 3C-vine
 208 models based on the Akaike information criterion \(AIC\). With the help of *CDVineCondFit* R function
 209 in “*CDVineCopulaConditional*” R package \(Bevacqua, 2017a\), based on the AIC, we selected the
 210 optimal tree structures \(i.e., detected the suitable variable ordering; seen in Figure 2\). ~~The selected
 211 bivariate copulas utilized in this study comprised Gaussian \(or Normal\), Student-t, Clayton, and
 212 Frank, as well as the corresponding survival functions. We used the R function *CDVineCondFit* in
 213 the “*CDVineCopulaConditional*” R package \(Bevacqua, 2017\), based on the Akaike information~~](#)

214 ~~critierion (AIC), to select the suitable bivariate copula for each pair of variables.~~

215 -----**Figure 2.**-----

216 A conditional copula density needs to be addressed in Equation 4, i.e., $G(y|\mathbf{w})$, where \mathbf{w} is a d -
 217 dimensional vector $\mathbf{w} = (w_1, \dots, w_d)$. Here, regarding the conditional distribution of y given the
 218 conditions \mathbf{w} , we introduced the h -function, $h(y, \mathbf{w}; \theta)$, to indicate the $G(y|\mathbf{w})$ as follows (Aas et al.,
 219 2009; Joe, 1996):

$$220 \quad h(y, \mathbf{w}; \theta) := G(y | \mathbf{w}) = \frac{\partial C_{y, w_j | \mathbf{w}_{-j}} [G(y | \mathbf{w}_{-j}), G(w_j | \mathbf{w}_{-j})]}{\partial G(w_j | \mathbf{w}_{-j})} \quad (5)$$

221 where θ denotes the parameter(s) of bivariate copula function $C_{y, w_j | \mathbf{w}_{-j}}$; w_j represents an arbitrary
 222 component of \mathbf{w} ; and \mathbf{w}_{-j} indicates the excluding element w_j from the vector \mathbf{w} .

223 Let the ordering variables be y_1, y_2 , and y_3 , the conditional variables be y_1 and y_2 , and the
 224 predictand be y_3 . Accordingly, the expression of $G(y_3|y_1, y_2)$, based on Equation 5, can be written as:

$$225 \quad G(y_3 | y_1, y_2) = \frac{\partial C_{z_3, z_1 | z_2} [G(y_3 | y_1), G(y_2 | y_1)]}{\partial G(y_2 | y_1)} = h \{ h(u_3 | u_1; \theta_{12}) | h(u_2 | u_1; \theta_{11}); \theta_{21} \} \quad (6)$$

226 where θ_{ij} (i denotes a tree and j is an edge) represents the parameters of different conditional copulas
 227 in the 3C-vine model (Figure 2a); and u_k ($k = 1, \dots, 3$) is the marginal cumulative distribution
 228 function (CDF) of y_k . The CDF for each variable is substituted by the [corresponding](#) empirical
 229 Gringorten cumulative probability (Bevacqua et al., 2017b; Genest et al., 2009; Wu et al., 2021a).

230 Here, we introduced the τ -th copula-quantile curve (Chen et al., 2009; Liu et al., 2018) to
 231 simulate u_3 based on Equation 6 and derived its inverse distribution function as follows:

$$232 \quad y_3 = N^{-1} \{ G(\tau | z_1, z_2) \} = N^{-1}(u_3) = N^{-1} \left[h^{-1} \left\{ h^{-1}(\tau | h(u_2 | u_1; \theta_{11}); \theta_{21}) | u_1; \theta_{12} \right\} \right] \quad (7)$$

233 where N^{-1} and h^{-1} signify the inverse form of Gaussian distribution and h -function, respectively; y_3
 234 is the forecasted agricultural drought ~~forecast~~ at time t (i.e., SSI_t); y_1 and y_2 are the predictors
 235 corresponding to the antecedent meteorological drought and agricultural drought persistence at time
 236 $t-i$ (i.e., SPI_{t-i} and SSI_{t-i}). The R functions of *BiCopHfunc* and *BiCopHinv* in the R package
 237 “*VineCopula*” (Nagler et al., 2021) were utilized to model the h -function and its inverse form for
 238 Equation 7, respectively.

239 The tree structure is related to the ordering variables, so when the ordering variables are $y_2, y_1,$
 240 and y_3 (conditional variables are y_1 and y_2 ; Figure 2b), Equations 6 and 7 can be changed analogously
 241 as:

$$242 \quad G(y_3 | y_2, y_1) = h \left\{ h(u_3 | u_2; \theta_{12}) | h(u_1 | u_2; \theta_{11}); \theta_{21} \right\} \quad (8)$$

$$243 \quad y_3 = N^{-1}(u_3) = N^{-1} \left[h^{-1} \left\{ h^{-1}(\tau | h(u_1 | u_2; \theta_{11}); \theta_{21}) | u_2; \theta_{12} \right\} \right] \quad (9)$$

244 With agricultural drought forecast via 3C-vine model, as the details presented in Figure 3, We
 245 we first selected the best 3C-vine model (i.e., selected the best model from Equations 7 and 9
 246 according to AIC). Then, generated a sample size of 1,000 uniformly distributed random values was
 247 generated over the interval $[0, 1]$ by Monte Carlo simulation. ~~Then Last~~, the best 3C-vine model (~~i.e.,~~
 248 ~~selected the best model from Equation 7 and Equation 9 according to AIC~~) was utilized to obtain
 249 1,000 simulations (or estimations) for y_3^{yr} . The best forecast of y_3^{yr} was finally calculated by the
 250 mean value of these simulations. Note that the leave-one-out cross validation (LOOCV) (Wilks,
 251 2014) is applied to forecast agricultural drought for each grid cell in August of every year during
 252 1961–2018 based on the 3C-vine or MG models, namely, each time one sample (or observation) was
 253 left for validation, and the rest were used to establish 3C-vine model or MG model and obtain the
 254 corresponding parameters of these models. In other words, this process was repeated 58 times (the

255 length of years used in this study) for a specific grid cell. ~~we applied the leave one out cross~~
 256 ~~validation (LOOCV) (Wilks, 2014) to forecast agricultural drought in August of every year during~~
 257 ~~1961–2018 for the 3C vine model or MG model, namely, the validation sample was left one in each~~
 258 ~~time, and the rest were used to establish the 3C vine model or MG model and obtain the~~
 259 ~~corresponding parameters.~~

260 -----Figure 3.-----

261 3.3. Performance metrics

262 Three evaluation metrics: ~~The~~ Nash-Sutcliffe efficiency (NSE), coefficient of determination
 263 (R^2), and root mean square error (RMSE), were utilized to assess the forecast performance of 3C-
 264 vine model ~~or~~ and MG model. These metrics can be expressed as:

$$265 \quad NSE = 1 - \frac{\sum_{i=1}^n (AP_i - AO_i)^2}{\sum_{i=1}^n (AO_i - \overline{AO})^2} \quad NSE \in (-\infty, 1] \quad (10)$$

$$266 \quad R^2 = \frac{\left[\sum_{i=1}^n (AO_i - \overline{AO})(AP_i - \overline{AP}) \right]^2}{\sum_{i=1}^n (AO_i - \overline{AO})^2 \cdot \sum_{i=1}^n (AP_i - \overline{AP})^2} \quad R^2 \in [0, 1] \quad (11)$$

$$267 \quad RMSE = \sqrt{\frac{1}{n} \sum_{i=1}^n (AP_i - AO_i)^2} \quad RMSE \in [0, +\infty) \quad (12)$$

268 where n is the number of forecast periods; AO_i and AP_i are the i -th observed and forecasted
 269 agricultural droughts (i.e., SSI), respectively; \overline{AO} and \overline{AP} denote the mean of the SSI
 270 observations and forecasts in the target month (e.g., August), respectively. Moreover, a most positive
 271 NSE and R^2 value and a lower RMSE value ~~expressed~~ indicate a good forecast performance for the

272 3C-vine model or MG model.

273 4. Results

274 4.1. Correlation patterns of agricultural drought with potential predictors

275 The dependence between variables can be measured by the correlation coefficient, indirectly
276 characterizing the quantity of common information between ~~the~~ two variables. ~~In this study, w~~We
277 employed Kendall's correlation coefficient (τ_k) to measure the dependence of agricultural drought at
278 current time t (SSI_t , herein t is August) with the previous meteorological drought (SPI_{t-i} , i indicates
279 the lag or lead time with 1–3-month herein) and agricultural drought persistence (SSI_{t-i}). It should
280 be mentioned that the significant correlation prevalent used may overestimate or overinterpret the
281 dependence between variables (Wilks, 2016). Therefore, we adopted the maximum false discovery
282 rate (FDR) of 0.1 to correct τ_k at the 0.05 significance level (Benjamini ~~&~~and Hochberg, 1995;
283 R othlisberger ~~&~~and Martius, 2019; Wilks, 2016).

284 -----**Figure 4.3.**-----

285 Figure ~~3~~4 summarizes 1–3-month lag τ_k between antecedent SPI (SSI) and succedent SSI for
286 August during 1961–2018 over China. For most regions of China under 1–3-month lag times, the
287 previous meteorological drought or agricultural drought persistence (memory) showed significant
288 positive correlations (i.e., the stippling in Figure 4) with the target agricultural drought (~~i.e., the~~
289 ~~stippling in Figure 3~~). Also, we found perfect agricultural drought memory over many regions of
290 China (excluding D4, a humid climate region) (Figures 4e and 4f~~3e and 3f~~), as the overlapping
291 information existed in SSI_t and SSI_{t-i} . Additionally, the dependency pattern varied temporally and
292 spatially, and this phenomenon evidently occurred with the lag (or lead) time extended, especially

293 between SPI_{t-i} and SSI_t (Figures [4a–4c](#)~~3a–3e~~). Overall, the prior meteorological drought and
294 agricultural drought memory provided reliable and useful forecast information for the subsequent
295 agricultural drought for most areas of China.

296 4.2. Forecast performance comparison between 3C-vine model and MG Model

297 We leveraged the MG model as a reference model to measure the performance of 3C-vine
298 model in forecasting ~~the~~ agricultural drought for the period 1961–2018 over China. Figures [5a–5i](#)
299 ~~4a–4i~~ show the difference in NSE , R^2 , and $RMSE$ between 3C-vine and MG models, i.e., $\Delta NSE =$
300 $NSE_{3C} - NSE_{MG}$, $\Delta R^2 = R^2_{3C} - R^2_{MG}$, and $\Delta RMSE = RMSE_{3C} - RMSE_{MG}$ under 1–3-month lead times for
301 August, respectively. ~~between the 3C-vine model and MG model with respect to NSE_{3C-MG} , R^2_{3C-}
302 MG , and $RMSE_{3C-MG}$ under 1–3-month leads for August, respectively.~~ In terms of the spatial extent
303 of $\Delta NSE > 0$ ~~$NSE_{3C-MG} > 0$~~ , $\Delta R^2 > 0$ ~~$R^2_{3C-MG} > 0$~~ , and $\Delta RMSE < 0$ ~~$RMSE_{3C-MG} < 0$~~ , the agricultural
304 drought forecast ability of 3C-vine model superior MG model was occupied 65%, 68%, and 58% of
305 land areas in China, respectively, under the 1-month lead SSI forecast (Figures [5a](#), [5d](#), and [5g](#)~~4a, 4d,~~
306 ~~and 4g~~), ~~except for western China (D3 and D7) and central China (D4)~~. The relationship between
307 predictors and the forecasted variable was simple under 1-month lead time, so the MG model better
308 showed their connection. However, with the lead time prolonged, the forecast skills of 3C-vine
309 model outperformed the MG model for most regions of China (e.g., Figures [5e](#) and [5f](#)~~4e and 4f,~~
310 accounting 72% and 74% of land areas in China for $\Delta R^2 > 0$ ~~$R^2_{3C-MG} > 0$~~ under 2–3-month lead times,
311 respectively). This indicates the 3C-vine model sufficiently utilized the forecasted information
312 contained by previous meteorological drought and agricultural drought persistence in comparison
313 with the MG model under the same conditions.

314 ~~It can be seen that~~ The forecast ability of 3C-vine model, compared with the MG model, is

315 limited over climate region D5 (e.g., Figures [5b](#) and [5c](#)~~4b and 4e~~). This may be related to the fact
316 that D5 is a crucial grain-producing region in China (Lu et al., 2012; Xiao et al., 2019; Zhang et al.,
317 2016), the intensive anthropogenic activities (e.g., irrigation and urbanization) may alter the linkage
318 between meteorological drought and agricultural drought, as well as the strength of agricultural
319 drought memory (AghaKouchak et al., 2021). To ensure food security, if D5 experiences a drought
320 event at the previous stage, agricultural managers and policymakers would mitigate the drought
321 through irrigation in a variety of ways, such as groundwater exploitation and reservoir operation
322 (Zhang et al., 2016). However, under this circumstance, the soil water obtaining the supplement
323 from the irrigation water would affect the performance of agricultural drought forecast.

324 -----**Figure 5.4.**-----

325 In contrast with the MG model, the 3C-vine model yielded a better forecast performance for
326 August under 1–3-month leads agricultural drought across most areas of China, except for the
327 climate region D5.

328 **4.3. Case study and sub-climate region assessment**

329 The severe drought hit most regions of China in summer 2018, especially in southern and
330 northern China, as the western North Pacific subtropical high abnormally impacted (Liu ~~&~~ [and](#) [Zhu](#),
331 2019; Zhang et al., 2020; Zhang et al., 2018). We chose the agricultural drought that occurred in
332 August of 2018 as a case study to investigate the forecast ability of 3C-vine model. Similarly, the
333 MG model was selected as a benchmark model. Figure [5-6](#) presents the SSI observations and 1–3-
334 month lead SSI forecasts for this agricultural drought using the 3C-vine model and MG model.
335 Obviously, the 1–3-month lead SSI forecasts via 3C-vine model resembled the observations (Figures
336 [6a–6d](#)~~5a–5d~~), which captured the droughts that emerged in southern China, northern China, and

337 northeastern China, i.e., climate regions D1–D2 and D4–D6. Comparing the 3C-vine model with
338 the MG model under 2–3-month leads (Figures [6c–6d](#) ~~5e–5d~~ versus Figures [6f–6g](#) ~~5f–5g~~), we
339 observed the deteriorating forecast skill of MG model in climate region D5, which tended to non-
340 drought state (i.e., $SSI > 0$), but the 3C-vine model better forecasted the agricultural drought for
341 these regions under the same conditions, although the severity of agricultural drought had some
342 decrement. The above analyses indicated that the 3C-vine model, using previous meteorological
343 drought and agricultural drought persistence as two predictors, had the ability for reliable drought
344 forecast over many regions of China.

345 -----Figure [6.5](#).-----

346 -----Figure [7.6](#).-----

347 Furthermore, to explore the skill of 3C-vine model in capturing the extremum of agricultural
348 drought (i.e., minimum and maximum SSIs), we randomly selected a typical region (black rectangle
349 boxes in Figure [6b](#) ~~5b~~) in each climate region. Note that these extreme SSI values were calculated
350 using the spatial average in each typical region. Figures [7a](#) and [7b](#) ~~6~~ shows the probability density
351 function (PDF) curve of minimum and maximum SSIs for these selected typical regions (D1S–D7S)
352 via the 3C-vine [model and MG](#) model for 1–3-month leads of August. Here, the vertical black dash
353 line denotes the SSI observation in each subplot. The x -axis value of peak point (i.e., high probability)
354 for each PDF curve is regarded as the best estimation of SSI under diverse lead times. [With the 3C-](#)
355 [vine model as an example \(analogously for the MG model\)](#), ~~For~~ [for](#) minimum SSI with 1–2-month
356 lead times, the difference between forecasted SSI and observed SSI was slight (except for D3S),
357 which all reflected the drought state for these typical regions (Figure [6a](#) ~~7a~~). The deteriorated skills
358 of 3C-vine [and MG](#) models in a typical region D3S may be attributed to the lengthy response time

359 existing between precipitation deficiency and soil moisture shortage, which is caused by the limited
360 precipitation that cannot effectively replenish the soil moisture depletion due to the incassation of
361 vadose zone. For the 3-month lead time, the poor forecasts were produced in a typical region D5S
362 for the minimum SSI. This phenomenon may result in the agricultural manager utilizing irrigation
363 to mitigate the effect of drought on crop growth, thus, the response relationship between
364 meteorological drought and agricultural drought accordingly would change (Xu et al., 2021**b**).

365 For the forecasted maximum SSI utilizing 3C-vine model ([analogously for the MG model](#)) over
366 diverse regions, the excellence forecast ability is displayed for the 1–3-month leads (Figure ~~6b~~[7b](#)),
367 excluding the typical regions D5S and D6S (PDF curve shifted left). For the abundant precipitation
368 and higher soil moisture content in D6S, the shortened response time between precipitation and soil
369 moisture (Xu et al., 2021**b**) may cause inferior forecasts of 3C-vine model for the target month.

370 [To display the robustness of 3C-vine model for forecasting agricultural drought in any month](#)
371 [of interest, we further forecasted extreme agricultural drought in July for D1S–D7S \(Figures 7c and](#)
372 [7d\). The difference between forecasted and observed extreme SSIs for the MG model is larger than](#)
373 [that of 3C-vine model in distinct typical regions, e.g., the forecasted maximum SSI in July on D4S](#)
374 [\(Figure 7d\). The width of PDF curve qualitatively provides an estimation of forecast uncertainty of](#)
375 [3C-vine model and MG model. As shown in Figure 7, in comparison with the 3C-vine model, we](#)
376 [found that the width of PDF curves in the MG model are broadened, indicating that the MG model](#)
377 [produced more pronounced uncertainty for agricultural drought forecast. Furthermore, the skills of](#)
378 [MG model tended to deteriorate over many selected typical regions, especially for 2–3-month lead](#)
379 [times of July and August. Generally, compared with the MG model under different lead times,](#)
380 [agricultural drought forecasts made by the 3C-vine model are more accurate across different typical](#)

381 [regions, in terms of predictive uncertainty \(i.e., the width of PDF curve\) as well as the difference](#)
382 [between observed and forecasted extreme SSIs \(Figures 7\).](#)

383 Moreover, to assess the forecast performance (according to NSE , R^2 , and $RMSE$) of the 3C-vine
384 model over each climate region, we counted the pixel contained in each climate region and
385 constructed the boxplots for these performance metrics (Figures [5j-514j-41](#)). We still selected the
386 MG model as the reference model, and obtained the difference between these two models, i.e.,
387 $\Delta NSE_{NSE_{3C-MG}}$, $\Delta R^2_{R^2_{3C-MG}}$, and $\Delta RMSE_{RMSE_{3C-MG}}$. The forecast performances of 3C-vine
388 model and MG model were generally consistent for 1-month lead of August over climate regions
389 D1–D7 (Figures [5j-514j-41](#), the median percentile of $\Delta NSE_{NSE_{3C-MG}}$, $\Delta R^2_{R^2_{3C-MG}}$,
390 ~~and $RMSE_{3C-MG}$~~ were all around the 0 line), indicating the improved skills of 3C-vine model was
391 limited under the same condition. Obviously, the median percentile of $\Delta NSE_{NSE_{3C-MG}}$ and $\Delta R^2_{R^2_{3C-MG}}$
392 ~~MG~~ were greater than 0 as well as $\Delta RMSE_{RMSE_{3C-MG}}$ was lower than 0, respectively, for 2–3-month
393 leads SSI forecast of August in different climate regions D1–D7 (except for D5), indicating that the
394 3C-vine model [shows a better performance than the MG model in forecasting agricultural drought](#)
395 [over diverse climate regions of China.](#) ~~more accurately forecasted agricultural drought than did the~~
396 ~~MG model in diverse climate regions.~~

397 In conclusion, based the ability of typical agricultural drought forecasted (Figure [65](#)) and
398 extremum agricultural drought captured in selected typical regions (Figure [76](#)) and the
399 comprehensive forecast performance showed in diverse climate regions (Figures [5j-514j-41](#)), the
400 3C-vine model had a good forecast skill for 1–3-month leads agricultural drought of August over
401 most areas of China.

402 **5. Discussion and Conclusions**

403 This study developed a C-vine copula model for forecasting agricultural drought over China
404 under three dimensions, in which antecedent meteorological drought and agricultural drought
405 persistence ~~at time $t-1$ (t denotes target month) was were primarily~~ employed as two predictors. We
406 selected the MG model as a competition model, in terms of the difference in NSE, R^2 , and RMSE
407 between 3C-vine and MG models, to evaluate the forecast performance of 3C-vine model. These
408 performance metrics all displayed that the 3C-vine model, especially for 2–3-month lead times,
409 outperformed the MG model in many climate regions over China (except for D5, which lies in humid
410 and subhumid regions of northern China) (Figure [54](#)). Compared with the MG model, the 3C-vine
411 model yielded a good forecast skill for the selected typical agricultural droughts (Figure 5). Besides,
412 the nearly perfect forecast of extremum agricultural drought in typical regions (Figure [76](#)) further
413 certified the excellent ability of 3C-vine model.

414 Heterogeneous topography and anthropogenic activities (e.g., irrigation and urbanization) have
415 certainly impacted precipitation interpolation and soil moisture simulation, which may depart from
416 the actual precipitation or soil moisture conditions, notwithstanding the precipitation of CN05.1 and
417 soil moisture of ERA5 ~~that~~ show good performances with respect to drought monitoring and
418 forecasting over China (Wang ~~&~~ [and](#) Yuan, 2021; Wu et al., 2021[a](#); Xu et al., 2009; Zhang et al.,
419 2021; Zhang et al., 2019). It can also influence the response (propagation) time ~~between~~ [from](#)
420 meteorological drought ~~and~~ [to](#) agricultural drought as well as agricultural drought memory and can
421 thus lead to the 3C-vine model falling short in some climate regions. To address this issue, we can
422 comprehensively utilize multiple reanalysis data sets, e.g., the precipitation and soil moisture data
423 in Global Land Data Assimilation System (GLDAS) and ERA5, to reduce the uncertainty resulting
424 from a single data source (Wang ~~&~~ [and](#) Yuan, 2021; Wu et al., 2021[a](#)). Currently, it is a challenge to

425 consider irrigation activities into agricultural drought forecasting, especially at large spatial scales.
426 In addition to antecedent precipitation deficit, air temperature, relative humidity, and
427 evapotranspiration may influence soil moisture budget. Moreover, from the perspective of driving
428 mechanisms, the effect of certain atmospheric circulation anomalies (e.g., El Niño-Southern
429 Oscillation (ENSO), Pacific Decadal Oscillation (PDO), and North Arctic Oscillation (NAO)) on
430 agricultural drought at regional and global scales can also be considered as predictors (Zhang et al.,
431 2021). Therefore, a more efficient space can be established by leveraging these predictors for
432 [forecasting](#) agricultural drought ~~forecasting~~.

433 In recent years, a myriad of extreme events, such as heatwaves and flash droughts, have swept
434 many regions around the globe. These extreme events have a rapid onset with a few days or weeks
435 and lead to devastating impacts on agricultural production, water resource security, and human well-
436 being (Wang ~~&~~ [and](#) Yuan, 2021; Yuan et al., 2019; Zscheischler et al., 2020). Therefore, agricultural
437 drought forecasting at finer temporal scales (e.g., weekly) is essential for agricultural managers and
438 policymakers to manage and plan water use. Yet, with limited spatiotemporal resolution and the
439 length of model sample, we temporally have not carried out agricultural drought forecasting at sub-
440 monthly or pentad temporal scales.

441 The limitation of this study is that we choose a ~~single~~ “best” model from two C-vine copula
442 candidate models (i.e., Figure 2) as the ideal forecast. However, as the inherent structural differences
443 (i.e., ordering variables are different), the utilized best model may underestimate the forecast
444 uncertainty (Liu et al., 2021[a](#)). Therefore, to reduce the predictive uncertainty and improve the
445 forecast performance, a multi-model combination technique (e.g., Bayesian model averaging (Liu
446 et al., 2021[a](#); Long et al., 2017)) can be considered to merge different C-vine copula candidate

447 models. Moreover, as we only pay attention to the C-vine copulas and several bivariate copula
448 functions, the other D-vine copulas or regular vine copulas, as well as a multitude of bivariate copula
449 families (Sadegh et al., 2017) can be investigated to establish the forecast model for agricultural
450 drought in the next work.

451 **Data availability**

452 The grided monthly precipitation data with a 0.25° spatial resolution was provided by the
453 CN05.1 (<http://data.cma.cn>) for the period of 1961–2018. The grided monthly soil moisture data
454 with three soil depths (0–7 cm, 7–28 cm, and 28–100 cm) from the European Center for Medium-
455 Range Weather Forecast (ECMWF) ERA5 reanalysis datasets are available at 1961–1978:
456 [https://cds.climate.copernicus.eu/cdsapp#!/dataset/reanalysis-era5-single-levels-monthly-means-](https://cds.climate.copernicus.eu/cdsapp#!/dataset/reanalysis-era5-single-levels-monthly-means-preliminary-back-extension?tab=overview)
457 [preliminary-back-extension?tab=overview](https://cds.climate.copernicus.eu/cdsapp#!/dataset/reanalysis-era5-single-levels-monthly-means-preliminary-back-extension?tab=overview) and 1979–2018:
458 [https://cds.climate.copernicus.eu/cdsapp#!/dataset/reanalysis-era5-single-levels-monthly-](https://cds.climate.copernicus.eu/cdsapp#!/dataset/reanalysis-era5-single-levels-monthly-means?tab=overview)
459 [means?tab=overview](https://cds.climate.copernicus.eu/cdsapp#!/dataset/reanalysis-era5-single-levels-monthly-means?tab=overview).

460 **Author contribution**

461 Haijiang Wu: Conceptualization, Methodology, Software, Visualization, Writing - original draft.
462 Xiaoling Su: [Writing - review & editing](#), Data curation, Validation, Investigation, Funding
463 acquisition, Supervision, Formal analysis. Vijay P. Singh: Writing - review & editing, Supervision.
464 Te Zhang: Formal analysis, Investigation. Jixia Qi: Data curation, Investigation. [Shengzhi Huang:](#)
465 [Writing - review & editing, Investigation.](#)

466 **Competing interests**

467 The authors declare that they have no conflict of interest.

468 **Acknowledgments**

469 [The authors would like to thank two anonymous reviewers for their constructive comments and](#)
470 [suggestions which contributed to improving the quality of the paper.](#) This study was financially
471 supported by the National Natural Science Foundation of China (Grants No. 51879222 and
472 52079111).

473 **References**

474 [Aas, K., and Berg, D.: Models for construction of multivariate dependence – a comparison study,](#)
475 [Eur. J. Financ., 15\(7-8\), 639–659, <https://doi.org/10.1080/13518470802588767>, 2009.](#)

476 [Aas, K., Czado, C., Frigessi, A., and Bakken, H.: Pair-copula constructions of multiple dependence.](#)
477 [Insur. Math. Econ., 44\(2\), 182–198. <https://doi.org/10.1016/j.insmatheco.2007.02.001>, 2009.](#)

478 [AghaKouchak, A., Mirchi, A., Madani, K., Di Baldassarre, G., Nazemi, A., Alborzi, A., Anjileli, H.,](#)
479 [Azarderakhsh, M., Chiang, F., Hassanzadeh, E., Huning, L. S., Mallakpour, I., Martinez, A.,](#)
480 [Mazdiyasn, O., Moftakhari, H., Norouzi, H., Sadegh, M., Sadeqi, D., Van Loon, A. F., and](#)
481 [Wanders, N.: Anthropogenic Drought: Definition, Challenges, and Opportunities, Rev.](#)
482 [Geophys., 59\(2\), e2019RG000683, <https://doi.org/10.1029/2019rg000683>, 2021.](#)

483 [Bedford, T., and Cooke, R. M.: Vines—A new graphical model for dependent random variables, Ann.](#)
484 [Stat., 30\(4\), 1031–1068, 2002.](#)

485 [Benjamini, Y., and Hochberg, Y.: Controlling the false discovery rate: A practical and powerful](#)
486 [approach to multiple testing, J. R. Stat. Soc. Ser. B-Stat. Methodol., 57\(1\), 289–300,](#)
487 [https://doi.org/10.1111/j.2517-6161.1995.tb02031.x, 1995.](#)

488 [Bevacqua, E.: CDVineCopulaConditional: Sampling from conditional C- and D-vine copulas, R](#)
489 [package, version 0.1.1, <https://CRAN.R-project.org/package=CDVineCopulaConditional>,](#)

490 [2017a.](#)

491 [Bevacqua, E., Maraun, D., Hobæk Haff, I., Widmann, M., and Vrac, M.: Multivariate statistical](#)
492 [modelling of compound events via pair-copula constructions: analysis of floods in Ravenna](#)
493 [\(Italy\), Hydrol. Earth Syst. Sci., 21\(6\), 2701–2723, \[https://doi.org/10.5194/hess-21-2701-\]\(https://doi.org/10.5194/hess-21-2701-2017\)](#)
494 [2017, 2017b.](#)

495 [Chen, X., Koenker, R., and Xiao, Z.: Copula-based nonlinear quantile autoregression, Econom. J.,](#)
496 [12, S50–S67, <https://doi.org/10.1111/j.1368-423X.2008.00274.x>, 2009.](#)

497 [Dißmann, J., Brechmann, E. C., Czado, C., and Kurowicka, D.: Selecting and estimating regular](#)
498 [vine copulae and application to financial returns, Comput. Stat. Data Anal., 59, 52–69,](#)
499 [https://doi.org/10.1016/j.csda.2012.08.010, 2013.](#)

500 [FAO: The impact of disasters and crises on agriculture and food security, Food and Agriculture](#)
501 [Organization of the United Nations, Rome, <https://doi.org/10.4060/cb3673en>, 2021.](#)

502 [Ganguli, P., and Reddy, M. J.: Ensemble prediction of regional droughts using climate inputs and](#)
503 [the SVM-copula approach, Hydrol. Process., 28\(19\), 4989–5009,](#)
504 [https://doi.org/10.1002/hyp.9966, 2014.](#)

505 [Genest, C., Rémillard, B., and Beaudoin, D.: Goodness-of-fit tests for copulas: A review and a power](#)
506 [study, Insur. Math. Econ., 44\(2\), 199–213, <https://doi.org/10.1016/j.insmatheco.2007.10.005>,](#)
507 [2009.](#)

508 [Gringorten, I. I.: A plotting rule for extreme probability paper, J. Geophys. Res., 68\(3\), 813–814,](#)
509 [https://doi.org/10.1029/JZ068i003p00813, 1963.](#)

510 [Hao, Z., Hao, F., Singh, V. P., Sun, A. Y., and Xia, Y.: Probabilistic prediction of hydrologic drought](#)
511 [using a conditional probability approach based on the meta-Gaussian model, J. Hydrol., 542,](#)
512 [772–780, <https://doi.org/10.1016/j.jhydrol.2016.09.048>, 2016.](#)

513 [Hao, Z., Hao, F., Singh, V. P., and Ouyang W.: Quantitative risk assessment of the effects of drought](#)
514 [on extreme temperature in eastern China, *J. Geophys. Res.-Atmos.*, 122, 9050–9059,](#)
515 <https://doi.org/10.1002/2017JD027030>, 2017.

516 [Hao, Z., Hao, F., Singh, V. P., and Zhang, X.: Statistical prediction of the severity of compound dry-](#)
517 [hot events based on El Niño-Southern Oscillation, *J. Hydrol.*, 572, 243–250.](#)
518 <https://doi.org/10.1016/j.jhydrol.2019.03.001>, 2019a.

519 [Hao, Z., Hao, F., Xia, Y., Singh, V. P., and Zhang, X.: A monitoring and prediction system for](#)
520 [compound dry and hot events, *Environ. Res. Lett.*, 14\(11\), 114034,](#)
521 <https://doi.org/10.1088/1748-9326/ab4df5>, 2019b.

522 [He, L., Hao, X., Li, H., and Han, T.: How Do Extreme Summer Precipitation Events Over Eastern](#)
523 [China Subregions Change? *Geophys. Res. Lett.*, 48, e2020GL091849,](#)
524 <https://doi.org/10.1029/2020GL091849>, 2021.

525 [Hemri, S., Lisniak, D., and Klein, B.: Multivariate postprocessing techniques for probabilistic](#)
526 [hydrological forecasting, *Water Resour. Res.*, 51\(9\), 7436–7451,](#)
527 <https://doi.org/10.1002/2014wr016473>, 2015.

528 [Joe, H.: Families of m-variate distributions with given margins and \$m\(m-1\)/2\$ bivariate dependence](#)
529 [parameters, *Institute of Mathematical Statistics Lecture Notes – Monograph Series*](#)
530 [Distributions with fixed marginals and related topics, 120–141,](#)
531 <https://doi.org/10.1214/lnms/1215452614>, 1996.

532 [Joe, H.: Dependence modeling with copulas, Chapman and Hall/CRC, 2014.](#)

533 [Lesk, C., Rowhani, P., and Ramankutty, N.: Influence of extreme weather disasters on global crop](#)
534 [production, *Nature*, 529\(7584\), 84–87, https://doi.org/10.1038/nature16467](#), 2016.

535 [Liu, B., and Zhu, C.: Extremely Late Onset of the 2018 South China Sea Summer Monsoon](#)

536 [Following a La Niña Event: Effects of Triple SST Anomaly Mode in the North Atlantic and a](#)
537 [Weaker Mongolian Cyclone, Geophys. Res. Lett., 46\(5\), 2956–2963,](#)
538 <https://doi.org/10.1029/2018gl081718>, 2019.

539 [Liu, Z., Cheng, L., Hao, Z., Li, J., Thorstensen, A., and Gao, H.: A Framework for Exploring Joint](#)
540 [Effects of Conditional Factors on Compound Floods, Water Resour. Res., 54\(4\), 2681–2696,](#)
541 <https://doi.org/10.1002/2017wr021662>, 2018.

542 [Liu, Z., Cheng, L., Lin, K., and Cai, H.: A hybrid bayesian vine model for water level prediction,](#)
543 [Environ. Modell. Softw., 142, 105075, https://doi.org/10.1016/j.envsoft.2021.105075, 2021a.](#)

544 [Liu, Z., Xie, Y., Cheng, L., Lin, K., Tu, X., and Chen, X.: Stability of spatial dependence structure](#)
545 [of extreme precipitation and the concurrent risk over a nested basin, J. Hydrol., 602, 126766,](#)
546 <https://doi.org/10.1016/j.jhydrol.2021.126766>, 2021b.

547 [Long, D., Bai, L., Yan, L., Zhang, C., Yang, W., Lei, H., Quan, J., Meng, X., and Shi, C.: Generation](#)
548 [of spatially complete and daily continuous surface soil moisture of high spatial resolution,](#)
549 [Remote Sens. Environ., 233, 111364, https://doi.org/10.1016/j.rse.2019.111364, 2019.](#)

550 [Long, D., Pan, Y., Zhou, J., Chen, Y., Hou, X., Hong, Y., Scanlon, B. R., and Longuevergne, L.:](#)
551 [Global analysis of spatiotemporal variability in merged total water storage changes using](#)
552 [multiple GRACE products and global hydrological models, Remote Sens. Environ., 192, 198–](#)
553 [216, https://doi.org/10.1016/j.rse.2017.02.011, 2017.](#)

554 [Lu, Y., Wu, K., Jiang, Y., Guo, Y., and Desneux, N.: Widespread adoption of Bt cotton and insecticide](#)
555 [decrease promotes biocontrol services, Nature, 487\(7407\), 362–365,](#)
556 <https://doi.org/10.1038/nature11153>, 2012.

557 [Ma, F., Luo, L., Ye, A., and Duan, Q.: Seasonal drought predictability and forecast skill in the semi-](#)
558 [arid endorheic Heihe River basin in northwestern China, Hydrol. Earth Syst. Sci., 22, 5697–](#)

5709, <https://doi.org/10.5194/hess-22-5697-2018>, 2018.

560 [Modanesi, S., Massari, C., Camici, S., Brocca, L., and Amarnath, G.: Do Satellite Surface Soil](#)
561 [Moisture Observations Better Retain Information About Crop-Yield Variability in Drought](#)
562 [Conditions? Water Resour. Res., 56\(2\), e2019WR025855,](#)
563 <https://doi.org/10.1029/2019wr025855>, 2020.

564 [Nagler, T., Schepsmeier, U., Stoeber, J., Brechmann, E. C., Graeler, B., Erhardt, T., Almeida, C.,](#)
565 [Min, A., Czado, C., Hofmann, M., Killiches, M., Joe, H. and Vatter, T.: VineCopula: Statistical](#)
566 [Inference of Vine Copulas, R Package Version 2.4.2, https://CRAN.R-](#)
567 <project.org/package=VineCopula>, 2021.

568 [Nelsen, R. B.: An Introduction to Copulas, 2nd ed., Springer, N. Y., 2013.](#)

569 [Orth, R., and Destouni, G.: Drought reduces blue-water fluxes more strongly than green-water fluxes](#)
570 [in Europe, Nat. Commun., 9\(1\), 3602, https://doi.org/10.1038/s41467-018-06013-7, 2018.](#)

571 [Röthlisberger, M., and Martius, O.: Quantifying the Local Effect of Northern Hemisphere](#)
572 [Atmospheric Blocks on the Persistence of Summer Hot and Dry Spells, Geophys. Res. Lett.,](#)
573 [46\(16\), 10101–10111, https://doi.org/10.1029/2019gl083745, 2019.](#)

574 [Sadegh, M., Ragno, E., and AghaKouchak, A.: Multivariate Copula Analysis Toolbox \(MvCAT\):](#)
575 [Describing dependence and underlying uncertainty using a Bayesian framework, Water Resour.](#)
576 [Res., 53\(6\), 5166–5183, https://doi.org/10.1002/2016wr020242, 2017.](#)

577 [Sarhadi, A., Burn, D. H., Concepción Ausín, M., and Wiper, M. P.: Time-varying nonstationary](#)
578 [multivariate risk analysis using a dynamic Bayesian copula, Water Resour. Res., 52\(3\), 2327–](#)
579 [2349, https://doi.org/10.1002/2015wr018525, 2016.](#)

580 [Su, B., Huang, J., Fischer, T., Wang, Y., Kundzewicz, Z. W., Zhai, J., Sun, H., Wang, A., Zeng, X.,](#)
581 [Wang, G., Tao, H., Gemmer, M., Li, X., and Jiang, T.: Drought losses in China might double](#)

582 [between the 1.5 degrees C and 2.0 degrees C warming, P. Natl. Acad. Sci. USA, 115\(42\),](#)
583 [10600–10605, https://doi.org/10.1073/pnas.1802129115, 2018.](#)

584 [Vernieuwe, H., Vandenberghe, S., De Baets, B., and Verhoest, N. E. C.: A continuous rainfall model](#)
585 [based on vine copulas, Hydrol. Earth Syst. Sci., 19\(6\), 2685–2699,](#)
586 [https://doi.org/10.5194/hess-19-2685-2015, 2015.](#)

587 [Wang, W., Dong, Z., Lall, U., Dong, N., and Yang, M.: Monthly Streamflow Simulation for the](#)
588 [Headwater Catchment of the Yellow River Basin With a Hybrid Statistical-Dynamical Model,](#)
589 [Water Resour. Res., 55\(9\), 7606–7621, https://doi.org/10.1029/2019wr025103, 2019.](#)

590 [Wang, Y., and Yuan, X.: Anthropogenic Speeding Up of South China Flash Droughts as Exemplified](#)
591 [by the 2019 Summer-Autumn Transition Season, Geophys. Res. Lett., 48\(9\), e2020GL091901,](#)
592 [https://doi.org/10.1029/2020gl091901, 2021.](#)

593 [Wilks, D. S.: Statistical methods in the atmospheric sciences, Academic Press, 2014.](#)

594 [Wilks, D. S.: “The Stippling Shows Statistically Significant Grid Points”: How Research Results are](#)
595 [Routinely Overstated and Overinterpreted, and What to Do about It, B. Am. Meteorol. Soc.,](#)
596 [97\(12\), 2263–2273, https://doi.org/10.1175/bams-d-15-00267.1, 2016.](#)

597 [Wu, H., Su, X., Singh, V. P., Feng, K., and Niu, J.: Agricultural Drought Prediction Based on](#)
598 [Conditional Distributions of Vine Copulas, Water Resour. Res., 57\(8\), e2021WR029562,](#)
599 [https://doi.org/10.1029/2021wr029562, 2021a.](#)

600 [Wu, H., Su, X., and Zhang, G.: Prediction of agricultural drought in China based on Meta-Gaussian](#)
601 [model, Acta Geogr. Sin., 76\(3\), 525–538, https://doi.org/10.11821/dlxb202103003, 2021b.](#)

602 [Wu, J., Chen, X., Yu, Z., Yao, H., Li, W., and Zhang, D.: Assessing the impact of human regulations](#)
603 [on hydrological drought development and recovery based on a ‘simulated-observed’](#)
604 [comparison of the SWAT model. J. Hydrol., 577, 123990,](#)

605 <https://doi.org/10.1016/j.jhydrol.2019.123990>, 2019.

606 [Wu, J., Gao, X., Giorgi, F., and Chen, D.: Changes of effective temperature and cold/hot days in late](#)
607 [decades over China based on a high resolution gridded observation dataset, *Int. J. Climatol.*,](#)
608 [37, 788–800, <https://doi.org/10.1002/joc.5038>, 2017.](#)

609 [Xiao, G., Zhao, Z., Liang, L., Meng, F., Wu, W., and Guo, Y.: Improving nitrogen and water use](#)
610 [efficiency in a wheat-maize rotation system in the North China Plain using optimized farming](#)
611 [practices, *Agric. Water Manage.*, 212, 172–180, <https://doi.org/10.1016/j.agwat.2018.09.011>,](#)
612 [2019.](#)

613 [Xiong, L., Yu, K.-x., and Gottschalk, L.: Estimation of the distribution of annual runoff from climatic](#)
614 [variables using copulas, *Water Resour. Res.*, 50\(9\), 7134–7152,](#)
615 [https://doi.org/10.1002/2013wr015159, 2014.](#)

616 [Xu, L., Chen, N., Chen, Z., Zhang, C., and Yu, H.: Spatiotemporal forecasting in earth system science:](#)
617 [Methods, uncertainties, predictability and future directions. *Earth-Sci. Rev.*, 222, 103828,](#)
618 [https://doi.org/10.1016/j.earscirev.2021.103828, 2021a.](#)

619 [Xu, Y., Gao, X., Shen, Y., Xu, C., Shi, Y., and Giorgi, F.: A daily temperature dataset over China and](#)
620 [its application in validating a RCM simulation, *Adv. Atmos. Sci.*, 26\(4\), 763–772,](#)
621 [https://doi.org/10.1007/s00376-009-9029-z, 2009.](#)

622 [Xu, Y., Zhang, X., Hao, Z., Singh, V. P., and Hao, F.: Characterization of agricultural drought](#)
623 [propagation over China based on bivariate probabilistic quantification, *J. Hydrol.*, 598, 126194,](#)
624 [https://doi.org/10.1016/j.jhydrol.2021.126194, 2021b.](#)

625 [Yao, N., Li, Y., Lei, T., and Peng, L.: Drought evolution, severity and trends in mainland China over](#)
626 [1961-2013, *Sci. Total Environ.*, 616–617, 73–89,](#)
627 [https://doi.org/10.1016/j.scitotenv.2017.10.327, 2018.](#)

628 [Yuan, X., Wang, L., Wu, P., Ji, P., Sheffield, J., and Zhang, M.: Anthropogenic shift towards higher](#)
629 [risk of flash drought over China, Nat. Commun., 10\(1\), 4661, \[https://doi.org/10.1038/s41467-\]\(https://doi.org/10.1038/s41467-019-12692-7\)](#)
630 [019-12692-7, 2019.](#)

631 [Zhang, J., Mu, Q., and Huang, J.: Assessing the remotely sensed Drought Severity Index for](#)
632 [agricultural drought monitoring and impact analysis in North China, Ecol. Indic., 63, 296–309,](#)
633 [https://doi.org/10.1016/j.ecolind.2015.11.062, 2016.](#)

634 [Zhang, L., and Singh, V. P.: Copulas and their applications in water resources engineering,](#)
635 [Cambridge University Press, 2019.](#)

636 [Zhang, L., Zhou, T., Chen, X., Wu, P., Christidis, N., and Lott, F. C.: The late spring drought of 2018](#)
637 [in South China, Bull. Amer. Meteorol. Soc., 101\(1\), S59–S64, \[https://doi.org/10.1175/BAMS-\]\(https://doi.org/10.1175/BAMS-D-19-0202.1\)](#)
638 [D-19-0202.1, 2020.](#)

639 [Zhang, Q., Qi, T., Singh, V. P., Chen, Y. D., and Xiao, M.: Regional Frequency Analysis of Droughts](#)
640 [in China: A Multivariate Perspective, Water Resour. Manag., 29\(6\), 1767–1787,](#)
641 [https://doi.org/10.1007/s11269-014-0910-x, 2015.](#)

642 [Zhang, Q., Li, Q., Singh, V. P., Shi, P., Huang, Q., and Sun, P.: Nonparametric integrated](#)
643 [agrometeorological drought monitoring: Model development and application, J. Geophys.](#)
644 [Res.-Atmos., 123, 73–88, <https://doi.org/10.1002/2017JD027448>, 2018.](#)

645 [Zhang, Q., Yu, H., Sun, P., Singh, V. P., and Shi, P.: Multisource data based agricultural drought](#)
646 [monitoring and agricultural loss in China, Glob. Planet. Change, 172, 298–306,](#)
647 [https://doi.org/10.1016/j.gloplacha.2018.10.017, 2019.](#)

648 [Zhang, T., Su, X., and Feng, K.: The development of a novel nonstationary meteorological and](#)
649 [hydrological drought index using the climatic and anthropogenic indices as covariates, Sci.](#)
650 [Total Environ., 786, 147385, <https://doi.org/10.1016/j.scitotenv.2021.147385>, 2021.](#)

651 [Zhang, X., Su, Z., Lv, J., Liu, W., Ma, M., Peng, J., and Leng, G.: A Set of Satellite-Based Near](#)
652 [Real-Time Meteorological Drought Monitoring Data over China, *Remote Sens.*, 11\(4\), 453,](#)
653 <https://doi.org/10.3390/rs11040453>, 2019.

654 [Zhang, Y., Hao, Z., Feng, S., Zhang, X., Xu, Y., and Hao, F.: Agricultural drought prediction in China](#)
655 [based on drought propagation and large-scale drivers, *Agric. Water Manage.*, 255, 107028,](#)
656 <https://doi.org/10.1016/j.agwat.2021.107028>, 2021.

657 [Zhang, Y., Wang, Z., Sha, S., and Feng, J.: Drought Events and Its Causes in Summer of 2018 in](#)
658 [China. *J. Arid Meteorol.*, 36\(5\), 884–892, https://doi.org/10.11755/j.issn.1006-7639\(2018\)-05-](#)
659 [0884](#), 2018.

660 [Zhao, S.: A new scheme for comprehensive physical regionalization in China, *Acta Geogr. Sin.*,](#)
661 [38\(1\), 1–10, 1983.](#)

662 [Zhou, S., Williams, A. P., Berg, A. M., Cook, B. I., Zhang, Y., Hagemann, S., Lorenz, R., Seneviratne,](#)
663 [S. I., and Gentine, P.: Land-atmosphere feedbacks exacerbate concurrent soil drought and](#)
664 [atmospheric aridity, *P. Natl. Acad. Sci. USA*, 116\(38\), 18848–18853,](#)
665 <https://doi.org/10.1073/pnas.1904955116>, 2019.

666 [Zscheischler, J., Martius, O., Westra, S., Bevacqua, E., Raymond, C., Horton, R. M., van den Hurk,](#)
667 [B., AghaKouchak, A., Jézéquel, A., Mahecha, M. D., Maraun, D., Ramos, A. M., Ridder, N.](#)
668 [N., Thiery, W., and Vignotto, E.: A typology of compound weather and climate events, *Nature*](#)
669 [Reviews Earth & Environment](#), 1(7), 333–347, <https://doi.org/10.1038/s43017-020-0060-z>,

670 [2020.](#)

671 ~~Aas, K. & Berg, D. (2009). Models for construction of multivariate dependence—a comparison~~
672 ~~study. *The European Journal of Finance*, 15(7–8), 639–659.~~
673 ~~<https://doi.org/10.1080/13518470802588767>~~

674 Aas, K., Czado, C., Frigessi, A. & Bakken, H. (2009). Pair copula constructions of multiple
675 dependence. *Insurance: Mathematics and Economics*, 44(2), 182–198.
676 <https://doi.org/10.1016/j.insmatheco.2007.02.001>

677 AghaKouchak, A., Mirchi, A., Madani, K., Di Baldassarre, G., Nazemi, A., Alborzi, A., et al. (2021).
678 Anthropogenic Drought: Definition, Challenges, and Opportunities. *Reviews of Geophysics*,
679 59(2), e2019RG000683. <https://doi.org/10.1029/2019rg000683>

680 Bedford, T. & Cooke, R. M. (2002). Vines—A new graphical model for dependent random variables.
681 *Annals of Statistics* 30(4), 1031–1068.

682 Benjamini, Y. & Hochberg, Y. (1995). Controlling the false discovery rate: A practical and powerful
683 approach to multiple testing. *Journal of the Royal Statistical Society*, 57(1), 289–300.
684 <https://doi.org/10.1111/j.2517-6161.1995.tb02031.x>

685 Bevacqua, E. (2017). CDVineCopulaConditional: Sampling from conditional C- and D-vine copulas,
686 R package, version 0.1.1. <https://CRAN.R-project.org/package=CDVineCopulaConditional>

687 Bevacqua, E., Maraun, D., Hobæk Haff, I., Widmann, M. & Vrac, M. (2017). Multivariate statistical
688 modelling of compound events via pair-copula constructions: analysis of floods in Ravenna
689 (Italy). *Hydrology and Earth System Sciences*, 21(6), 2701–2723. [https://doi.org/10.5194/hess-](https://doi.org/10.5194/hess-21-2701-2017)
690 [21-2701-2017](https://doi.org/10.5194/hess-21-2701-2017)

691 Chen, X., Koenker, R. & Xiao, Z. (2009). Copula-based nonlinear quantile autoregression.
692 *Econometrics Journal*, 12, S50–S67. <https://doi.org/10.1111/j.1368-423X.2008.00274.x>

693 FAO. (2021). The impact of disasters and crises on agriculture and food security. *Food and*
694 *Agriculture Organization of the United Nations, Rome*. <https://doi.org/10.4060/cb3673en>

695 Ganguli, P. & Reddy, M. J. (2014). Ensemble prediction of regional droughts using climate inputs
696 and the SVM-copula approach. *Hydrological Processes*, 28(19), 4989–5009.

697 <https://doi.org/10.1002/hyp.9966>

698 Genest, C., Rémillard, B. & Beaudoin, D. (2009). Goodness-of-fit tests for copulas: A review and a
699 power study. *Insurance: Mathematics and Economics*, 44(2), 199-213.
700 <https://doi.org/10.1016/j.insmatheco.2007.10.005>

701 Gringorten, I. I. (1963). A plotting rule for extreme probability paper. *Journal of Geophysical*
702 *Research*, 68(3), 813-814. <https://doi.org/10.1029/JZ068i003p00813>

703 Hao, Z., Hao, F., Singh, V. P., Sun, A. Y. & Xia, Y. (2016). Probabilistic prediction of hydrologic
704 drought using a conditional probability approach based on the meta-Gaussian model. *Journal*
705 *of Hydrology*, 542, 772-780. <https://doi.org/10.1016/j.jhydrol.2016.09.048>

706 Hao, Z., Hao, F., Singh, V. P. & Ouyang W. (2017). Quantitative risk assessment of the effects of
707 drought on extreme temperature in eastern China. *Journal of Geophysical Research:*
708 *Atmosphere*, 122, 9050-9059, <https://doi.org/10.1002/2017JD027030>

709 Hao, Z., Hao, F., Singh, V. P. & Zhang, X. (2019). Statistical prediction of the severity of compound
710 dry-hot events based on El Niño-Southern Oscillation. *Journal of Hydrology*, 572, 243-250.
711 <https://doi.org/10.1016/j.jhydrol.2019.03.001>

712 Hao, Z., Hao, F., Xia, Y., Singh, V. P. & Zhang, X. (2019). A monitoring and prediction system for
713 compound dry and hot events. *Environmental Research Letters*, 14(11), 114034.
714 <https://doi.org/10.1088/1748-9326/ab4df5>

715 He, L., Hao, X., Li, H. & Han, T. (2021). How Do Extreme Summer Precipitation Events Over
716 Eastern China Subregions Change? *Geophysical Research Letters*, 48, e2020GL091849.
717 <https://doi.org/10.1029/2020GL091849>

718 Hemri, S., Lisniak, D. & Klein, B. (2015). Multivariate postprocessing techniques for probabilistic
719 hydrological forecasting. *Water Resources Research*, 51(9), 7436-7451.

- 720 <https://doi.org/10.1002/2014wr016473>
- 721 Joe, H. (1996). Families of m -variate distributions with given margins and $m(m-1)/2$ bivariate
722 dependence parameters. Distributions with fixed marginals and related topics. *Institute of*
723 *Mathematical Statistics Lecture Notes Monograph Series*, 28, 120-141.
724 <https://doi.org/10.1214/lnms/1215452614>
- 725 Joe, H. (2014). Dependence modeling with copulas. Chapman and Hall/CRC.
- 726 Lesk, C., Rowhani, P. & Ramankutty, N. (2016). Influence of extreme weather disasters on global
727 crop production. *Nature*, 529(7584), 84-87. <https://doi.org/10.1038/nature16467>
- 728 Liu, B. & Zhu, C. (2019). Extremely Late Onset of the 2018 South China Sea Summer Monsoon
729 Following a La Niña Event: Effects of Triple SST Anomaly Mode in the North Atlantic and a
730 Weaker Mongolian Cyclone. *Geophysical Research Letters*, 46(5), 2956-2963.
731 <https://doi.org/10.1029/2018gl081718>
- 732 Liu, Z., Cheng, L., Hao, Z., Li, J., Thorstensen, A. & Gao, H. (2018). A Framework for Exploring
733 Joint Effects of Conditional Factors on Compound Floods. *Water Resources Research*, 54(4),
734 2681-2696. <https://doi.org/10.1002/2017wr021662>
- 735 Liu, Z., Cheng, L., Lin, K. & Cai, H. (2021). A hybrid bayesian vine model for water level prediction.
736 *Environmental Modelling & Software*, 142, 105075.
737 <https://doi.org/10.1016/j.envsoft.2021.105075>
- 738 Liu, Z., Xie, Y., Cheng, L., Lin, K., Tu, X. & Chen, X. (2021). Stability of spatial dependence
739 structure of extreme precipitation and the concurrent risk over a nested basin. *Journal of*
740 *Hydrology*, 602, 126766. <https://doi.org/10.1016/j.jhydrol.2021.126766>
- 741 Long, D., Bai, L., Yan, L., Zhang, C., Yang, W., Lei, H., et al. (2019). Generation of spatially
742 complete and daily continuous surface soil moisture of high spatial resolution. *Remote Sensing*

743 *of Environment*, 233, 111364. <https://doi.org/10.1016/j.rse.2019.111364>

744 Long, D., Pan, Y., Zhou, J., Chen, Y., Hou, X., Hong, Y., et al. (2017). Global analysis of
745 spatiotemporal variability in merged total water storage changes using multiple GRACE
746 products and global hydrological models. *Remote Sensing of Environment*, 192, 198–216.
747 <https://doi.org/10.1016/j.rse.2017.02.011>

748 Lu, Y., Wu, K., Jiang, Y., Guo, Y. & Desneux, N. (2012). Widespread adoption of Bt cotton and
749 insecticide decrease promotes biocontrol services. *Nature*, 487(7407), 362–365.
750 <https://doi.org/10.1038/nature11153>

751 Modanesi, S., Massari, C., Camici, S., Brocca, L. & Amarnath, G. (2020). Do Satellite Surface Soil
752 Moisture Observations Better Retain Information About Crop Yield Variability in Drought
753 Conditions? *Water Resources Research*, 56(2), e2019WR025855.
754 <https://doi.org/10.1029/2019wr025855>

755 Nagler, T., Schepsmeier, U., Stoeber, J., Brechmann, E. C., Graeler, B., Erhardt, T., et al. (2021).
756 VineCopula: Statistical Inference of Vine Copulas, R Package Version 2.4.2.
757 <https://CRAN.R-project.org/package=VineCopula>

758 Nelsen, R. B. (2013). *An Introduction to Copulas*. 2nd ed., Springer, N. Y.

759 Orth, R. & Destouni, G. (2018). Drought reduces blue water fluxes more strongly than green water
760 fluxes in Europe. *Nature Communications*, 9(1), 3602. [https://doi.org/10.1038/s41467-018-](https://doi.org/10.1038/s41467-018-06013-7)
761 [06013-7](https://doi.org/10.1038/s41467-018-06013-7)

762 Röthlisberger, M. & Martius, O. (2019). Quantifying the Local Effect of Northern Hemisphere
763 Atmospheric Blocks on the Persistence of Summer Hot and Dry Spells. *Geophysical Research*
764 *Letters*, 46(16), 10101–10111. <https://doi.org/10.1029/2019gl083745>

765 Sadegh, M., Ragno, E. & AghaKouchak, A. (2017). Multivariate Copula Analysis Toolbox

766 ~~(MvCAT): Describing dependence and underlying uncertainty using a Bayesian framework.~~
767 ~~*Water Resources Research*, 53(6), 5166-5183. <https://doi.org/10.1002/2016wr020242>~~

768 ~~Sarhadi, A., Burn, D. H., Concepción Ausín, M. & Wiper, M. P. (2016). Time-varying nonstationary~~
769 ~~multivariate risk analysis using a dynamic Bayesian copula. *Water Resources Research*, 52(3),~~
770 ~~2327-2349. <https://doi.org/10.1002/2015wr018525>~~

771 ~~Su, B., Huang, J., Fischer, T., Wang, Y., Kundzewicz, Z. W., Zhai, J., et al. (2018). Drought losses~~
772 ~~in China might double between the 1.5 degrees C and 2.0 degrees C warming. *Proceedings of*~~
773 ~~*the National Academy of Sciences of the United States of America*, 115(42), 10600-10605.~~
774 ~~<https://doi.org/10.1073/pnas.1802129115>~~

775 ~~Vernieuwe, H., Vandenberghe, S., De Baets, B. & Verhoest, N. E. C. (2015). A continuous rainfall~~
776 ~~model based on vine copulas. *Hydrology and Earth System Sciences*, 19(6), 2685-2699.~~
777 ~~<https://doi.org/10.5194/hess-19-2685-2015>~~

778 ~~Wang, W., Dong, Z., Lall, U., Dong, N. & Yang, M. (2019). Monthly Streamflow Simulation for the~~
779 ~~Headwater Catchment of the Yellow River Basin With a Hybrid Statistical-Dynamical Model.~~
780 ~~*Water Resources Research*, 55(9), 7606-7621. <https://doi.org/10.1029/2019wr025103>~~

781 ~~Wang, Y. & Yuan, X. (2021). Anthropogenic Speeding Up of South China Flash Droughts as~~
782 ~~Exemplified by the 2019 Summer-Autumn Transition Season. *Geophysical Research Letters*,~~
783 ~~48(9), e2020GL091901. <https://doi.org/10.1029/2020gl091901>~~

784 ~~Wilks, D. S. (2014). *Statistical methods in the atmospheric sciences*. Academic Press.~~

785 ~~Wilks, D. S. (2016). “The Stippling Shows Statistically Significant Grid Points”: How Research~~
786 ~~Results are Routinely Overstated and Overinterpreted, and What to Do about It. *Bulletin of the*~~
787 ~~*American Meteorological Society*, 97(12), 2263-2273. [https://doi.org/10.1175/bams-d-15-](https://doi.org/10.1175/bams-d-15-00267.1)~~
788 ~~[00267.1](https://doi.org/10.1175/bams-d-15-00267.1)~~

789 Wu, H., Su, X., Singh, V. P., Feng, K. & Niu, J. (2021). Agricultural Drought Prediction Based on
790 Conditional Distributions of Vine Copulas. *Water Resources Research*, 57(8),
791 e2021WR029562. <https://doi.org/10.1029/2021wr029562>

792 Wu, H., Su, X. & Zhang, G. (2021). Prediction of agricultural drought in China based on Meta-
793 Gaussian model. *Acta Geographica Sinica*, 76(3), 525-538.
794 <https://doi.org/10.11821/dlxb202103003>

795 Wu, J., Gao, X., Giorgi, F. & Chen, D. (2017). Changes of effective temperature and cold/hot days
796 in late decades over China based on a high-resolution gridded observation dataset.
797 *International Journal of Climatology*, 37, 788-800. <https://doi.org/10.1002/joc.5038>

798 Xiao, G., Zhao, Z., Liang, L., Meng, F., Wu, W. & Guo, Y. (2019). Improving nitrogen and water
799 use efficiency in a wheat-maize rotation system in the North China Plain using optimized
800 farming practices. *Agricultural Water Management*, 212, 172-180.
801 <https://doi.org/10.1016/j.agwat.2018.09.011>

802 Xiong, L., Yu, K. x. & Gottschalk, L. (2014). Estimation of the distribution of annual runoff from
803 climatic variables using copulas. *Water Resources Research*, 50(9), 7134-7152.
804 <https://doi.org/10.1002/2013wr015159>

805 Xu, Y., Gao, X., Shen, Y., Xu, C., Shi, Y. & Giorgi, F. (2009). A daily temperature dataset over China
806 and its application in validating a RCM simulation. *Advances in Atmospheric Sciences*, 26(4),
807 763-772. <https://doi.org/10.1007/s00376-009-9029-z>

808 Xu, Y., Zhang, X., Hao, Z., Singh, V. P. & Hao, F. (2021). Characterization of agricultural drought
809 propagation over China based on bivariate probabilistic quantification. *Journal of Hydrology*,
810 598, 126194. <https://doi.org/10.1016/j.jhydrol.2021.126194>

811 Yao, N., Li, Y., Lei, T. & Peng, L. (2018). Drought evolution, severity and trends in mainland China

812 over 1961–2013. *Science of the Total Environment*, 616–617, 73–89.
813 <https://doi.org/10.1016/j.scitotenv.2017.10.327>

814 Yuan, X., Wang, L., Wu, P., Ji, P., Sheffield, J. & Zhang, M. (2019). Anthropogenic shift towards
815 higher risk of flash drought over China. *Nature Communications*, 10(1), 4661.
816 <https://doi.org/10.1038/s41467-019-12692-7>

817 Zhang, J., Mu, Q. & Huang, J. (2016). Assessing the remotely sensed Drought Severity Index for
818 agricultural drought monitoring and impact analysis in North China. *Ecological Indicators*, 63,
819 296–309. <https://doi.org/10.1016/j.ecolind.2015.11.062>

820 Zhang, L. & Singh, V. P. (2019). Copulas and their applications in water resources engineering.
821 Cambridge University Press.

822 Zhang, L., Zhou, T., Chen, X., Wu, P., Christidis, N. & Lott, F. C. (2020). The late spring drought of
823 2018 in South China. *Bulletin of the American Meteorological Society*, 101(1), S59–S64.
824 <https://doi.org/10.1175/BAMS-D-19-0202.1>

825 Zhang, Q., Qi, T., Singh, V. P., Chen, Y. D. & Xiao, M. (2015). Regional Frequency Analysis of
826 Droughts in China: A Multivariate Perspective. *Water Resources Management*, 29(6), 1767–
827 1787. <https://doi.org/10.1007/s11269-014-0910-x>

828 Zhang, Q., Li, Q., Singh, V. P., Shi, P., Huang, Q. & Sun, P. (2018). Nonparametric integrated
829 agrometeorological drought monitoring: Model development and application. *Journal of*
830 *Geophysical Research: Atmospheres*, 123, 73–88. <https://doi.org/10.1002/2017JD027448>

831 Zhang, Q., Yu, H., Sun, P., Singh, V. P. & Shi, P. (2019). Multisource data based agricultural drought
832 monitoring and agricultural loss in China. *Global and Planetary Change*, 172, 298–306.
833 <https://doi.org/10.1016/j.gloplacha.2018.10.017>

834 Zhang, T., Su, X. & Feng, K. (2021). The development of a novel nonstationary meteorological and

835 hydrological drought index using the climatic and anthropogenic indices as covariates. *Science*
836 *of the Total Environment*, 786, 147385. <https://doi.org/10.1016/j.scitotenv.2021.147385>

837 Zhang, X., Su, Z., Lv, J., Liu, W., Ma, M., Peng, J., et al. (2019). A Set of Satellite-Based Near Real-
838 Time Meteorological Drought Monitoring Data over China. *Remote Sensing*, 11(4), 453.
839 <https://doi.org/10.3390/rs11040453>

840 Zhang, Y., Hao, Z., Feng, S., Zhang, X., Xu, Y. & Hao, F. (2021). Agricultural drought prediction in
841 China based on drought propagation and large-scale drivers. *Agricultural Water Management*,
842 255, 107028. <https://doi.org/10.1016/j.agwat.2021.107028>

843 Zhang, Y., Wang, Z., Sha, S. & Feng, J. (2018). Drought Events and Its Causes in Summer of 2018
844 in China. *Journal of Arid Meteorology*, 36(5), 884-892. [https://doi.org/10.11755/j.issn.1006-7639\(2018\)-05-0884](https://doi.org/10.11755/j.issn.1006-7639(2018)-05-0884)

845

846 Zhao, S. (1983). A new scheme for comprehensive physical regionalization in China. *Acta*
847 *Geographica Sinica*, 38(1), 1-10.

848 Zhou, S., Williams, A. P., Berg, A. M., Cook, B. I., Zhang, Y., Hagemann, S., et al. (2019). Land-
849 atmosphere feedbacks exacerbate concurrent soil drought and atmospheric aridity.
850 *Proceedings of the National Academy of Sciences of the United States of America*, 116(38),
851 18848-18853. <https://doi.org/10.1073/pnas.1904955116>

852 Zscheischler, J., Martius, O., Westra, S., Bevacqua, E., Raymond, C., Horton, R. M., et al. (2020).
853 A typology of compound weather and climate events. *Nature Reviews Earth & Environment*,
854 1(7), 333-347. <https://doi.org/10.1038/s43017-020-0060-z>

855

Figure Captions

857 **Figure 1.** Seven sub-climate regions division over China. The specific information of climate
858 regions D1–D7 is listed at the left-bottom in the panel.

859 **Figure 2.** Different schematic (two types) of C-vine copulas under three-dimensional scenarios. For
860 the first type (a), the ordering variables are y_1 , y_2 , and y_3 , while for the second type (b) that
861 are y_2 , y_1 , and y_3 . $C_{12}(C_{21})$, $C_{13}(C_{23})$, and $C_{23|1}(C_{13|2})$ denotes bivariate copulas with
862 parameters θ_{11} , θ_{12} , and θ_{21} , respectively. Here, θ_{ij} signifies the parameters of the j -th edge
863 with respect to the i -th tree. $G(\bullet|\bullet)$ denote conditional distribution functions.

864 **Figure 3.** [Flowchart of agricultural drought forecasting based on canonical vine copulas \(3C-vine\)](#)
865 [and meta-Gaussian \(MG\) model under three-dimensional scenarios.](#) Here, t denotes the
866 [target month \(e.g., August\); \$i\$ signifies the lead times \(1–3-months\); LOOCV is the](#)
867 [abbreviation of leave-one-out cross validation; \$y_1^{-yr}\(y_2^{-yr}\)\$ indicates the series after](#)
868 [removing a sample \(\$y_1^{yr}\(y_2^{yr}\)\$ \) for a specific year; and \$y_3^{yr}\$ is the agricultural drought forecast](#)
869 [value for the target month of a specific year. Note that the optimal tree structure \(\$i\$ or \$ii\$ on](#)
870 [the right-hand side of this figure\) is selected based on AIC to forecast agricultural drought.](#)

871 **Figure 34.** Spatial patterns of 1–3-months lag Kendall's correlation coefficient (τ_k) between SPI_{t-i}
872 and SSI_t (t denotes August, and i is 1–3-month lag time) (top row), as well as SSI_{t-i} and SSI_t
873 (bottom row) for August during 1961–2018 over China. Note the stippling indicates where
874 τ_k is at a 0.05 significance level, which is corrected via the false discovery rate (FDR) of
875 0.1.

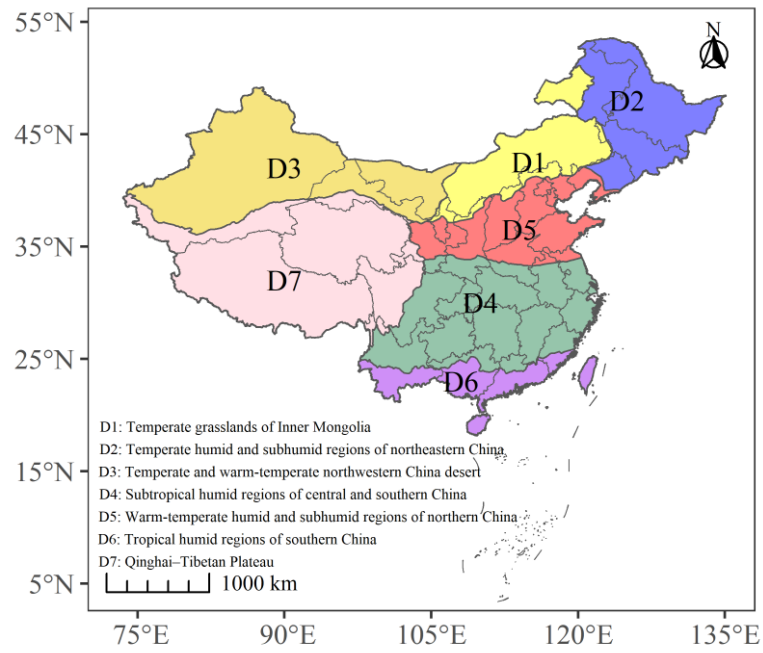
876 **Figure 45.** [Forecast performance based on \(a–c\) \$\Delta NSE\$ \(difference of \$NSE\$ between 3C-vine and MG](#)
877 [models, \$NSE_{3C}-NSE_{MG}\$ \), \(d–f\) \$\Delta R^2\$ \(\$R^2_{3C}-R^2_{MG}\$ \), and \(g–i\) \$\Delta RMSE\$ \(\$RMSE_{3C}-RMSE_{MG}\$ \) for](#)

878 the 1–3-month leads of August during 1961–2018 over China. The corresponding boxplots
879 of (j) ΔNSE , (k) ΔR^2 , and (l) $\Delta RMSE$ relative to a threshold of 0 (horizontal black dash line)
880 for agricultural drought forecast in August under 1–3-month leads in climate regions D1–
881 D7 over China. The percentage of $\Delta NSE > 0$, $\Delta R^2 > 0$, and $\Delta RMSE < 0$ is listed in the left-
882 bottom of corresponding sub-figure, respectively. Forecast performance of the 3C-vine
883 model based on (a–c) NSE_{3C-MG} (difference of NSE between 3C-vine model and MG
884 model), (d–f) R^2_{3C-MG} (difference of R^2 between 3C-vine and MG models), and (g–i)
885 $RMSE_{3C-MG}$ (difference in RMSE between 3C-vine and MG models) for the 1–3-month
886 leads of August during 1961–2018 over China. The corresponding boxplots of (j) NSE_{3C-
887 MG , (k) R^2_{3C-MG} , and (l) $RMSE_{3C-MG}$ relative to a threshold of 0 (horizontal black dash line)
888 for agricultural drought forecast in August under 1–3-month leads in climate regions D1–
889 D7 over China. The percentage of $NSE_{3C-MG} > 0$, $R^2_{3C-MG} > 0$, and $RMSE_{3C-MG} < 0$ is listed
890 in the left-bottom of corresponding sub-figure, respectively.

891 **Figure 56.** SSI observations in August of 2018 (a) as well as the corresponding SSI forecasts under
892 1–3-month lead times utilizing 3C-vine model (b–d) and MG model (e–g) over China. The
893 black rectangle boxes (as shown in b) denote the typical regions (corresponding to signify
894 D1S–D7S) selected in climate regions D1–D7.

895 **Figure 67.** Probability density function (PDF) curve of (a and c) minimum and (b and d) maximum
896 SSI under 1–3-month lead times for August and July during the 1961–2018 period over
897 seven selected typical regions in climate regions D1–D7 (i.e., these black rectangle boxes
898 in Figure 6b correspond to signify D1S–D7S, respectively). Black dash line and text
899 indicate the minimum and maximum observations of SSI in August and July over D1S–

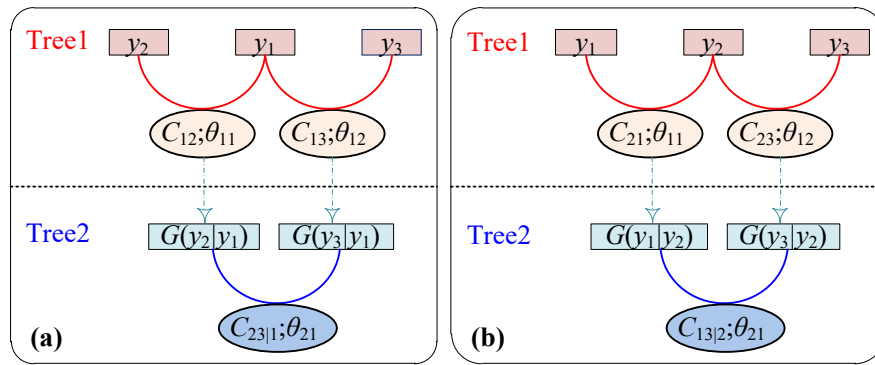
900 D7S. These texts with red (green), blue (yellow), and cyan (coral) colors of left (right) in
901 each sub-figure are SSI forecasts under 1–3-month lead times of August or July via 3C-
902 vine model (MG model), which correspond to the abscissa projected by the peak point of
903 each PDF. Probability density function (PDF) curve of (a) minimum and (b) maximum SSI
904 under 1–3-month lead times for August during the 1961–2018 period over seven selected
905 typical regions in climate regions D1–D7 (i.e., these black rectangle boxes in Figure 5b
906 correspond to signify D1S–D7S, respectively). Black dash line and text indicate the (a)
907 minimum and (b) maximum observations of SSI in D1S–D7S. These texts with red, blue,
908 and cyan colors of top right in each sub-figure are SSI forecasts under 1–3-month lead
909 times of August, which correspond to the abscissa projected by the peak point of each PDF.



910

911 **Figure 1.** Seven sub-climate regions division over China. The specific information of climate

912 regions D1–D7 is listed at the left-bottom in the panel.



913

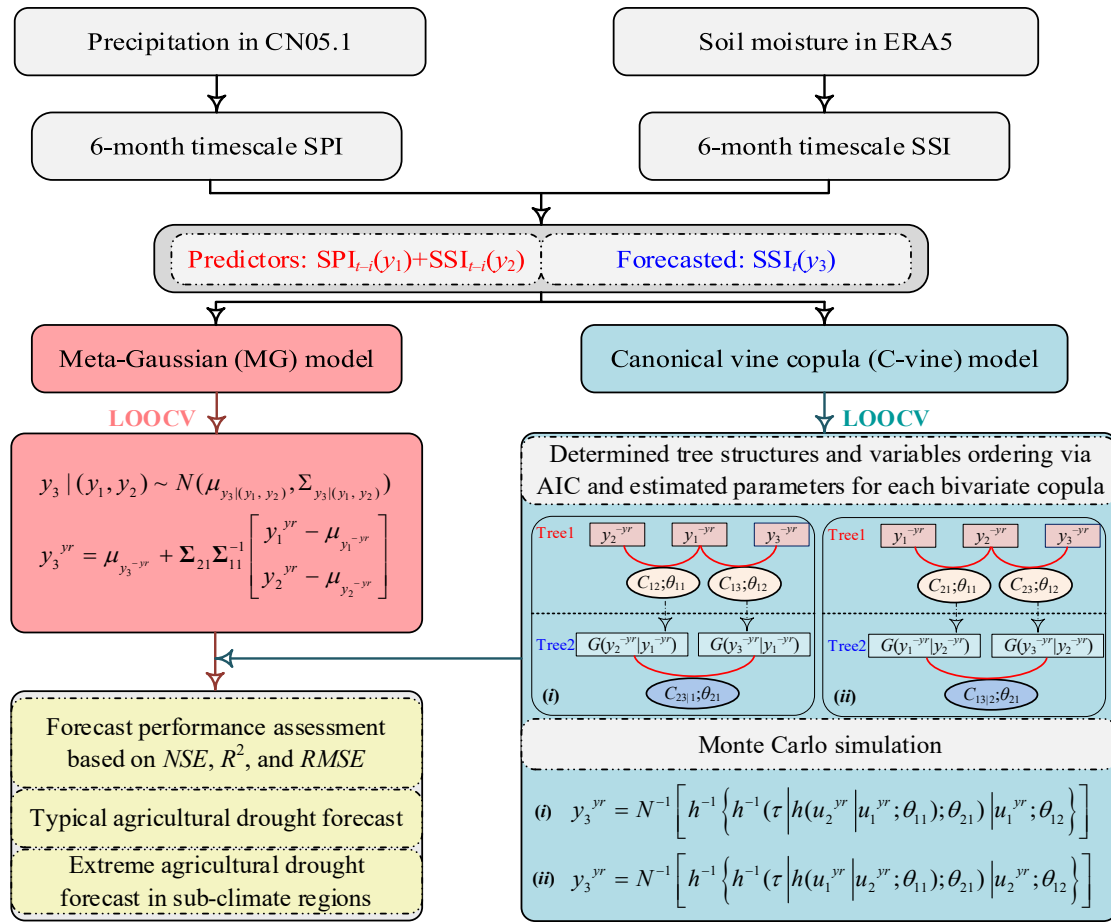
914 **Figure 2.** Different schematic (two types) of C-vine copulas under three-dimensional scenarios. For

915 the first type (a), the ordering variables are $y_1, y_2,$ and $y_3,$ while for the second type (b) that are $y_2, y_1,$

916 and $y_3.$ $C_{12}(C_{21}), C_{13}(C_{23}),$ and $C_{23|1}(C_{13|2})$ denotes bivariate copulas with parameters $\theta_{11}, \theta_{12},$ and $\theta_{21},$

917 respectively. Here, θ_{ij} signifies the parameters of the j -th edge with respect to the i -th tree. $G(\bullet|\bullet)$

918 denote conditional distribution functions.



919

920

921

922

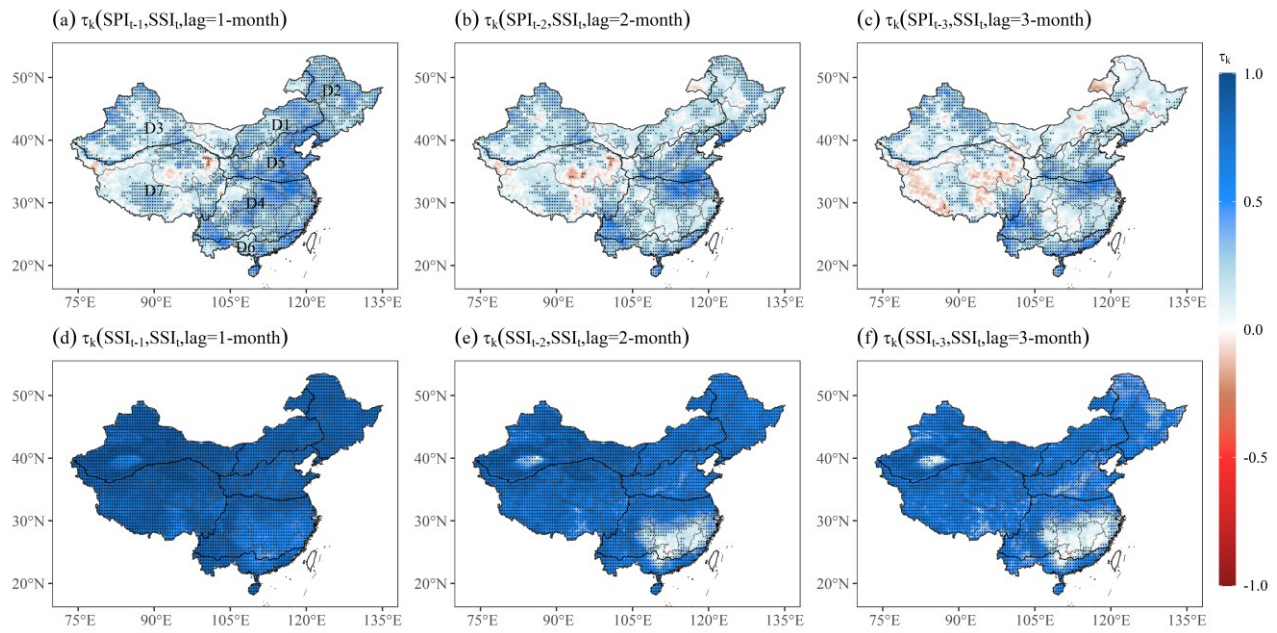
923

924

925

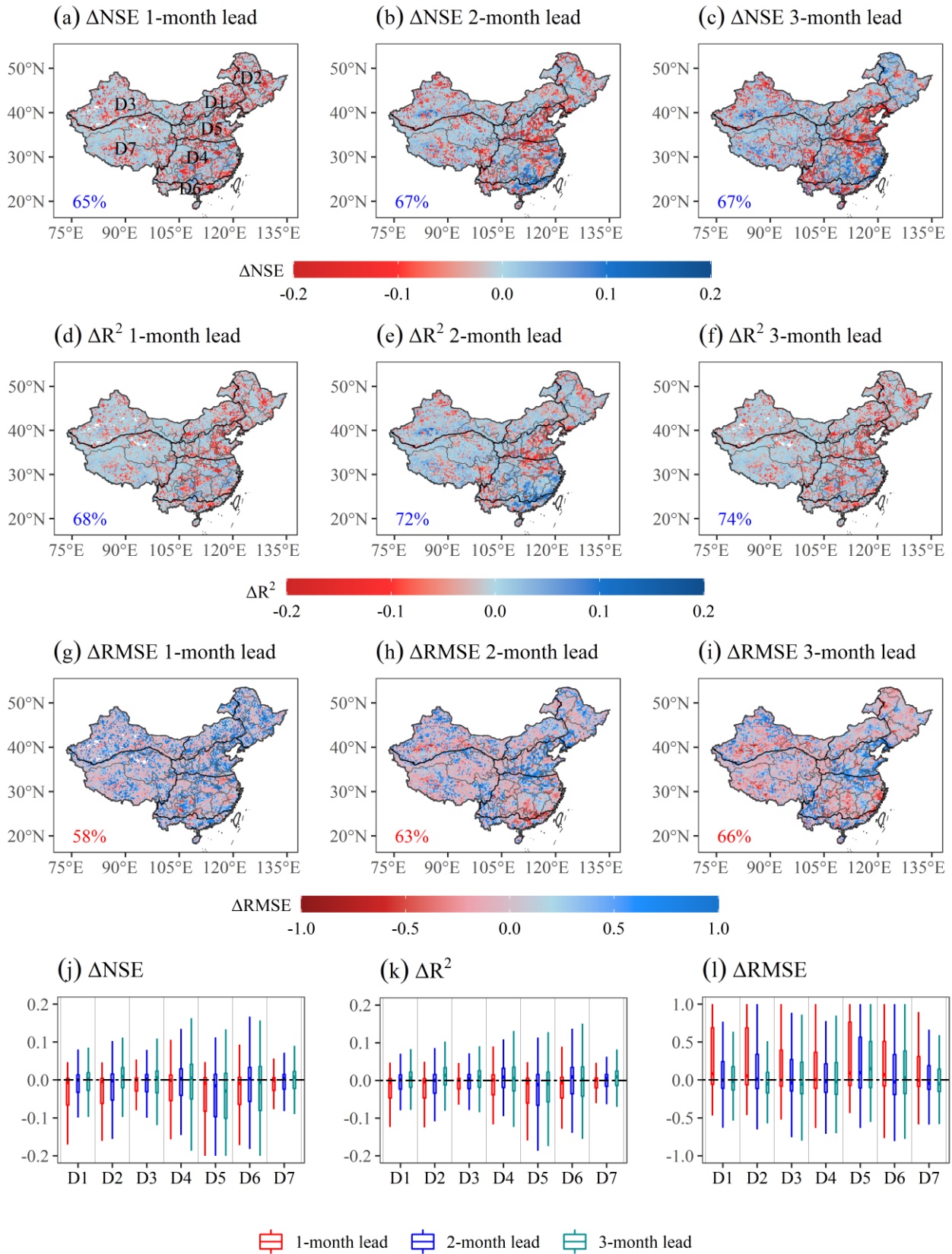
926

Figure 3. Flowchart of agricultural drought forecasting based on canonical vine copulas (3C-vine) and meta-Gaussian (MG) model under three-dimensional scenarios. Here, t denotes the target month (e.g., August); i signifies the lead times (1–3-months); LOOCV is the abbreviation of leave-one-out cross validation; $y_1^{-yr}(y_2^{-yr})$ indicates the series after removing a sample ($y_1^{yr}(y_2^{yr})$) for a specific year; and y_3^{yr} is the agricultural drought forecast value for the target month of a specific year. Note that the optimal tree structure (i or ii on the right-hand side of this figure) is selected based on AIC to forecast agricultural drought.



927

928 **Figure 34.** Spatial patterns of 1–3-months lag Kendall's correlation coefficient (τ_k) between SPI_{t-i}
 929 and SSI_t (t denotes August, and i is 1–3-month lag time) (top row), as well as SSI_{t-i} and SSI_t (bottom
 930 row) for August during 1961–2018 over China. Note the stippling indicates where τ_k is at a 0.05
 931 significance level, which is corrected via the false discovery rate (FDR) of 0.1.



932

933 **Figure 5.** Forecast performance based on (a–c) ΔNSE (difference of NSE between 3C-vine and

934 MG models, $NSE_{3C} - NSE_{MG}$), (d–f) ΔR^2 ($R^2_{3C} - R^2_{MG}$), and (g–i) $\Delta RMSE$ ($RMSE_{3C} - RMSE_{MG}$) for the

935 1–3-month leads of August during 1961–2018 over China. The corresponding boxplots of (j) ΔNSE ,
936 (k) ΔR^2 , and (l) $\Delta RMSE$ relative to a threshold of 0 (horizontal black dash line) for agricultural
937 drought forecast in August under 1–3-month leads in climate regions D1–D7 over China. The
938 percentage of $\Delta NSE > 0$, $\Delta R^2 > 0$, and $\Delta RMSE < 0$ is listed in the left-bottom of corresponding sub-
939 figure, respectively.

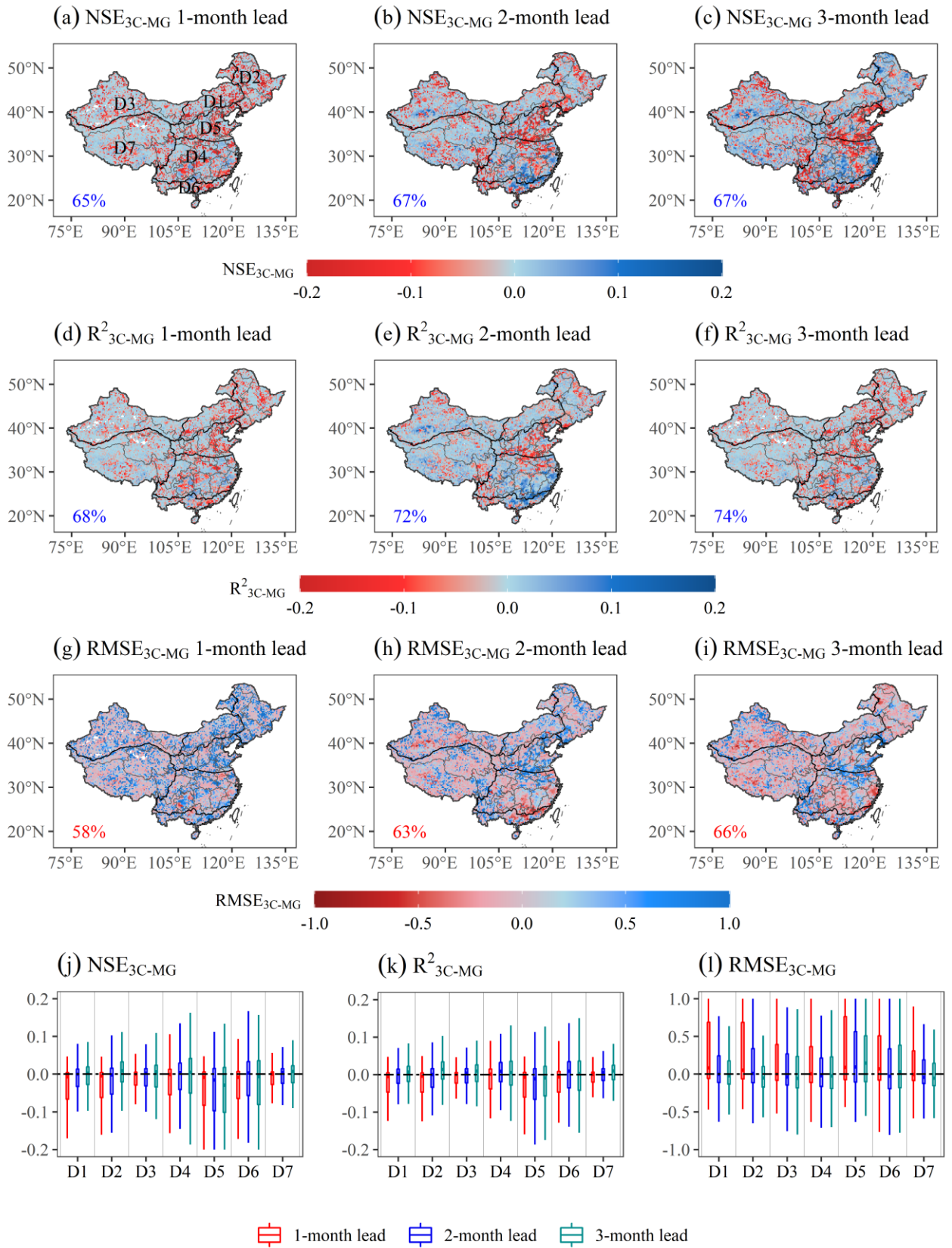
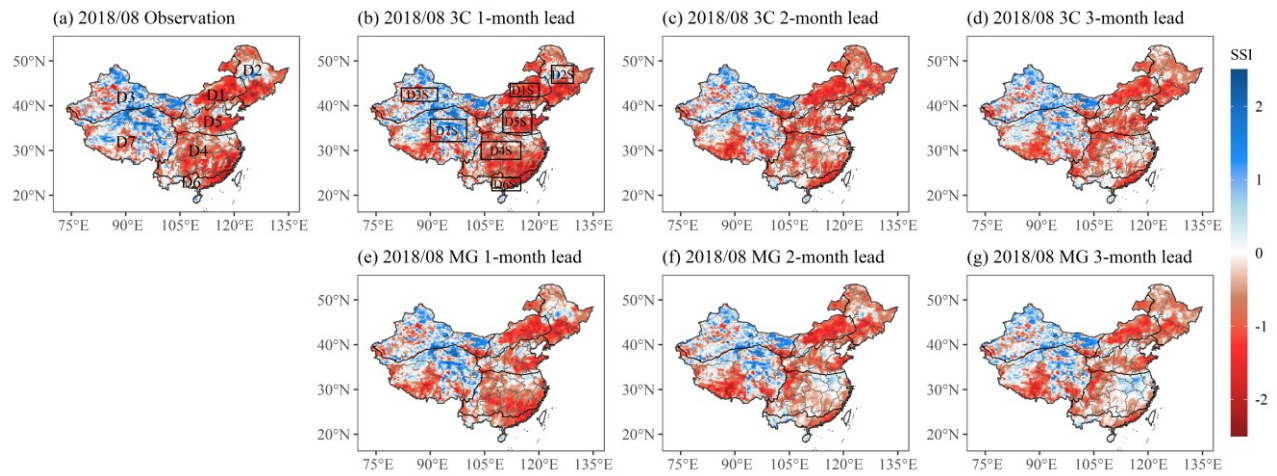


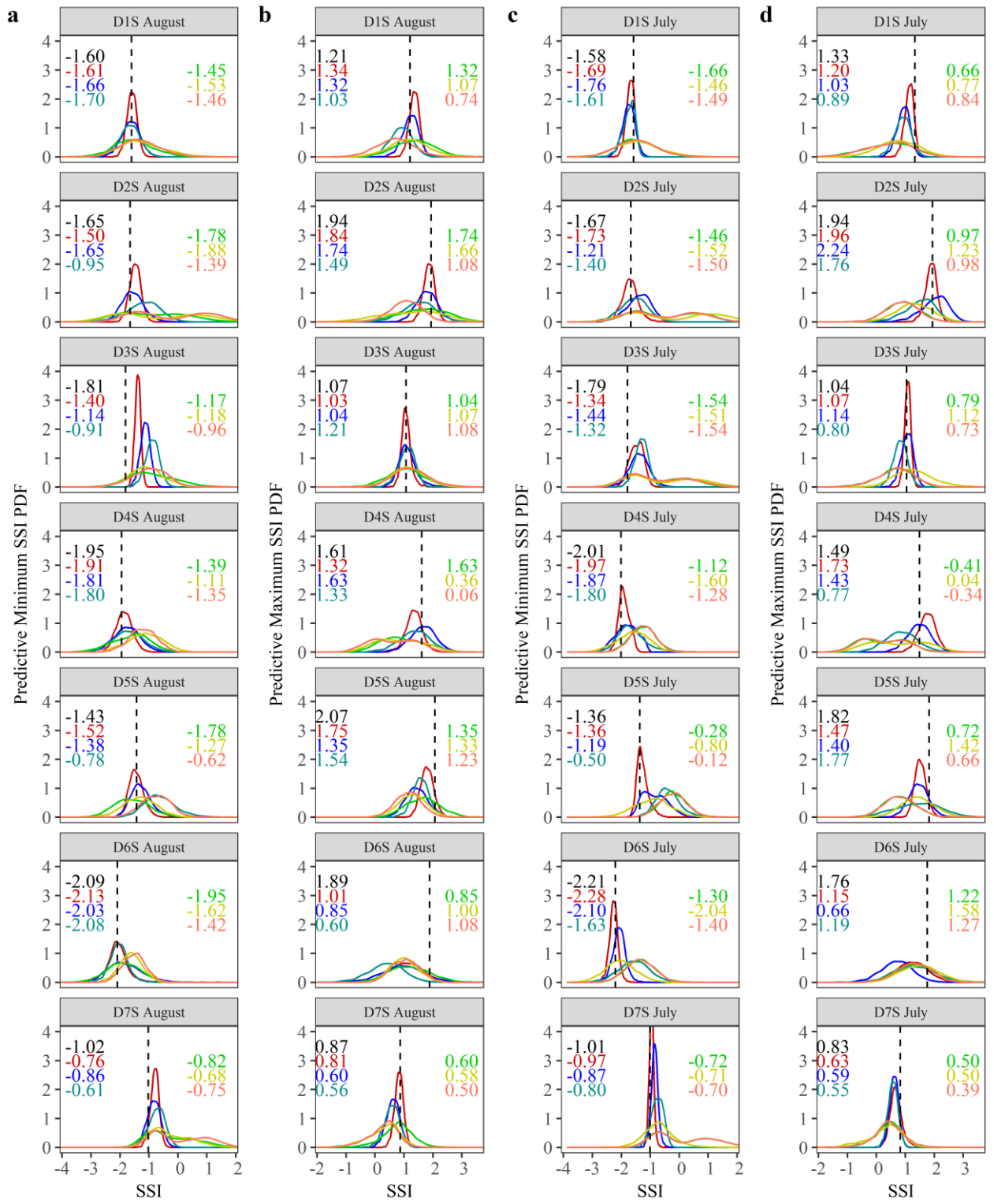
Figure 4. Forecast performance of the 3C-vine model based on (a-c) NSE_{3C-MG} (difference of NSE

943 between 3C vine model and MG model), (d–f) R^2_{3C-MG} (difference of R^2 between 3C vine and MG
944 models), and (g–i) $RMSE_{3C-MG}$ (difference in RMSE between 3C vine and MG models) for the 1–
945 3-month leads of August during 1961–2018 over China. The corresponding boxplots of (j) NSE_{3C-}
946 MG , (k) R^2_{3C-MG} , and (l) $RMSE_{3C-MG}$ relative to a threshold of 0 (horizontal black dash line) for
947 agricultural drought forecast in August under 1–3-month leads in climate regions D1–D7 over China.
948 The percentage of $NSE_{3C-MG} > 0$, $R^2_{3C-MG} > 0$, and $RMSE_{3C-MG} < 0$ is listed in the left bottom of
949 corresponding sub-figure, respectively.



950

951 **Figure 56.** SSI observations in August of 2018 (a) as well as the corresponding SSI forecasts under
 952 1–3-month lead times utilizing 3C-vine model (b–d) and MG model (e–g) over China. The black
 953 rectangle boxes (as shown in b) denote the typical regions (corresponding to signify D1S–D7S)
 954 selected in climate regions D1–D7.



— 3C 1-month lead — 3C 2-month lead — 3C 3-month lead — MG 1-month lead — MG 2-month lead — MG 3-month lead

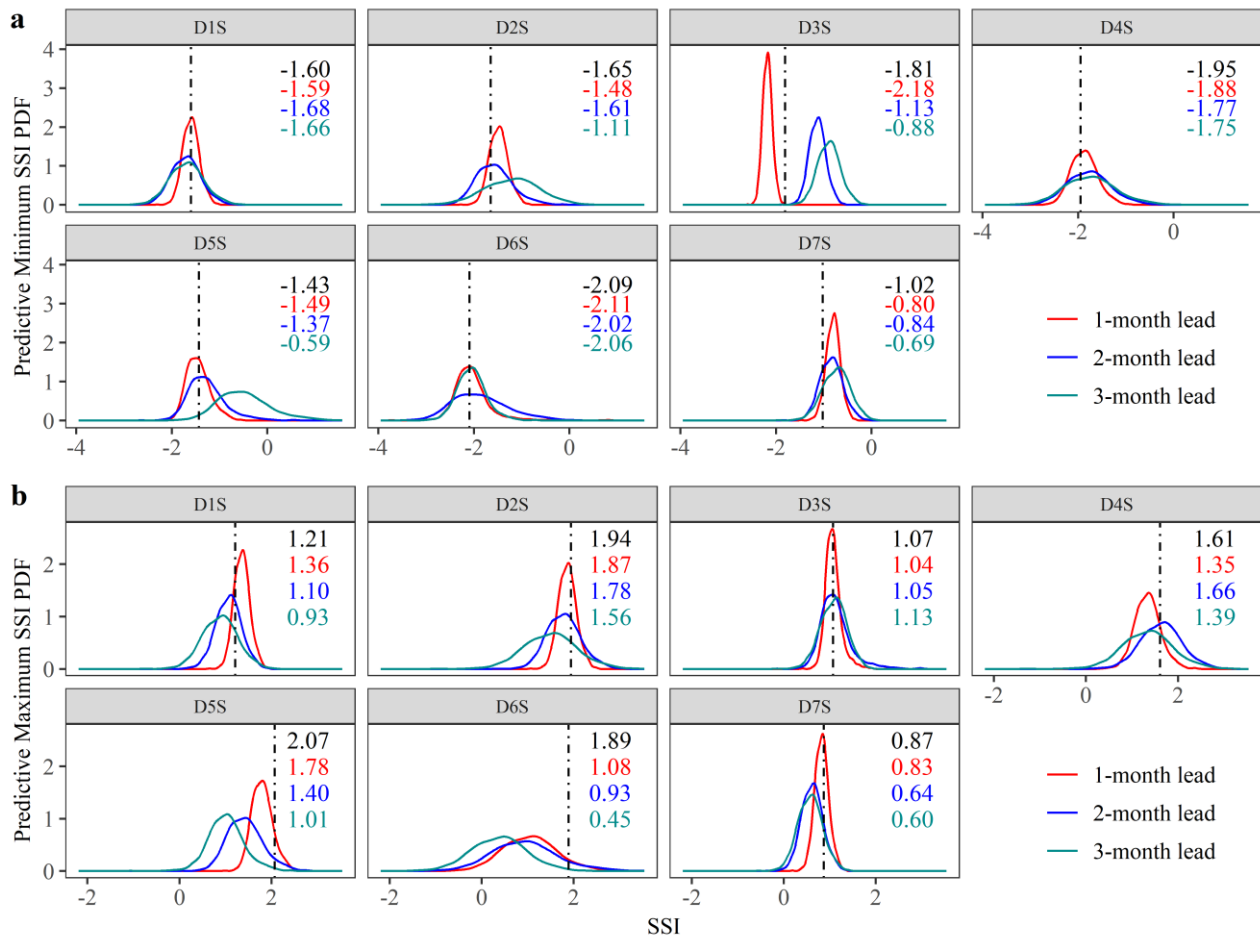
955

956 **Figure 7.** Probability density function (PDF) curve of (a and c) minimum and (b and d) maximum

957 SSI under 1–3-month lead times for August and July during the 1961–2018 period over seven

958 selected typical regions in climate regions D1–D7 (i.e., these black rectangle boxes in Figure 6b

959 correspond to signify D1S–D7S, respectively). Black dash line and text indicate the minimum and
 960 maximum observations of SSI in August and July over D1S–D7S. These texts with red (green), blue
 961 (yellow), and cyan (coral) colors of left (right) in each sub-figure are SSI forecasts under 1–3-month
 962 lead times of August or July via 3C-vine model (MG model), which correspond to the abscissa
 963 projected by the peak point of each PDF.



964 **Figure 6.** Probability density function (PDF) curve of (a) minimum and (b) maximum SSI under 1–
 965 3-month lead times for August during the 1961–2018 period over seven selected typical regions in
 966 climate regions D1–D7 (i.e., these black rectangle boxes in Figure 5b correspond to signify D1S–
 967 D7S, respectively). Black dash line and text indicate the (a) minimum and (b) maximum
 968 observations of SSI in D1S–D7S. These texts with red, blue, and cyan colors of top right in each
 969 sub-figure are SSI forecasts under 1–3-month lead times of August, which correspond to the abscissa
 970 projected by the peak point of each PDF.
 971